At 3 h after coronary ligation, 40 rats survived (78% survival rate); 30 were randomized to receive an intravenous injection of MSCs (MSC group, $n = 14$) or PBS (control group, $n = 16$), and 10 received fluorescence-labeled MSCs for examination of MSC differentiation ($n = 5$) and incorporation ($n = 5$). Eleven rats underwent a sham operation consisting of thoracotomy and cardiac exposure but without coronary artery ligation. At 3 h after coronary ligation, we administered 5×10^6 MSCs/100 μl in PBS or PBS alone through a catheter inserted into the left jugular vein in ~30 s. The subsequent mortality for 4 wk was 25% in the control group and 14% in the MSC group. This protocol resulted in the creation of three groups: normal rats given PBS (sham group, $n = 11$), myocardial infarction rats given PBS (control group, $n = 12$), and myocardial infarction rats given MSCs (MSC group, $n = 12$).

Expansion of bone marrow MSCs. MSC expansion was performed according to previously described methods (18). Briefly, we killed the male Lewis rats and harvested the bone marrow by flushing the cavity of the femurs and tibias with PBS. Bone marrow cells were introduced into 100-mm dishes and cultured in α-MEM supplemented with 10% FBS and antibiotics. A small number of cells developed visible symmetrical colonies by *day 5–7*. Nonadherent hematopoietic cells were removed, and the medium was replaced. The adherent, spindle-shaped MSC population expanded to $>5 \times 10^7$ cells by approximately four to five passages after the cells were first cultured.

Flow cytometry. Adherent cells were analyzed by fluorescence-activated cell sorting (FACS SCAN flow cytometer, Becton Dickinson). Cells were incubated for 30 min at 4 C with the FITC-conjugated mouse monoclonal antibodies against rat CD34 (clone ICO-115, Santa Cruz Biotechnology) and CD45 and CD90 (clones OX-1 and OX-7, respectively, Becton Dickinson). FITC-conjugated hamster anti-rat CD29 monoclonal antibody (clone Ha2/5, Becton Dickinson) and rabbit anti-rat c-Kit polyclonal antibody (clone C-19, Santa Cruz Biotechnology) were used. Isotype-identical antibodies served as controls.

Echocardiographic studies. Echocardiographic studies were performed by an investigator blinded to treatment allocation 4 wk after coronary ligation. Two-dimensional targeted M-mode traces were obtained at the level of the papillary muscles using an echocardiographic system equipped with a 7.5-MHz phased-array transducer (SONOS 5500, Hewlett-Packard, Andover, MA). Anterior and posterior end-diastolic wall thickness and left ventricular (LV) end-diastolic and end-systolic dimensions were measured by the American Society for Echocardiology leading-edge method from at least three consecutive cardiac cycles. LV fractional shortening was calculated as follows: $(LVD_d - LVD_s)/LVD_d \times 100$, where LVD_d is LV diastolic dimension and LVD_s is LV systolic dimension. LV volume and ejection fraction were calculated on the basis of the Teichholtz formula.

Hemodynamic studies. Hemodynamic studies were performed 4 wk after coronary ligation. A 1.5-Fr micromanometer-tipped catheter (Millar Instruments) was inserted in the right carotid artery for measurement of mean arterial pressure. Then the catheter was advanced into the LV for measurement of LV pressure. Hemodynamic variables were measured using a pressure transducer (model P23 ID, Gould) connected to a polygraph. After completion of these measurements, the left and right ventricles were excised and weighed. Infarction size was determined as a percentage of the entire LV area, as reported previously (8). Briefly, incisions were made in the LV, so that the tissue could be pressed flat. The circumference of the entire flat LV and the visualized infarcted area, as judged from the epicardial and endocardial sides, was outlined on a clear plastic sheet. The difference in weight between the two marked areas on the sheet was used to determine infarction size and was expressed as a percentage of LV surface area.

Histological examination. To detect fibrosis in cardiac muscle, the LV myocardium ($n = 5$ each group) was fixed in 10% formalin, cut transversely, embedded in paraffin, and stained with Masson's trichrome. To detect capillary endothelial cells in the peri-infarct area, samples of the harvested muscle ($n = 5$ each) were embedded in OCT compound (Miles Scientific), snap frozen in liquid nitrogen, and cut into transverse sections. Tissue sections were stained for alkaline phosphatase with an indoxyltetrazolium method. The number of capillary vessels was counted in the peri-infarct area using a light microscope at ×200 magnification. The numbers in five high-power fields were averaged and expressed as the number of capillary vessels. These morphometric studies were performed by two examiners who were blinded to treatment.

An additional five rats were used to examine whether transplanted MSCs differentiated into cardiomyocytes or vascular endothelial cells. Suspended MSCs were labeled with fluorescent dyes with a PKH-26 red fluorescent cell linker kit (Sigma Chemical, St. Louis, MO) before implantation, as reported previously (13). Fluorescence-labeled MSCs were intravenously administered 3 h after coronary ligation. This subgroup of rats was killed 4 wk after coronary ligation. After the LV was excised and dissected free, muscle samples were embedded in OCT compound, snap frozen in liquid nitrogen, and cut into sections. Immunofluorescent staining for cardiac and endothelial cell markers was performed using monoclonal mouse antidesmin (Dako), anti-cardiac troponin T (Novo), anticonnexin43 (Sigma Chemical), and polyclonal rabbit anti-von Willebrand factor (Dako). FITC-conjugated IgG antibody (BD Pharmingen and Molecular Probes) was used as a secondary antibody.

At 24 h after intravenous administration of PKH-26-labeled MSCs, cardiac muscle was embedded in OCT compound and snap frozen in liquid nitrogen. Then the cardiac muscle from base to apex was

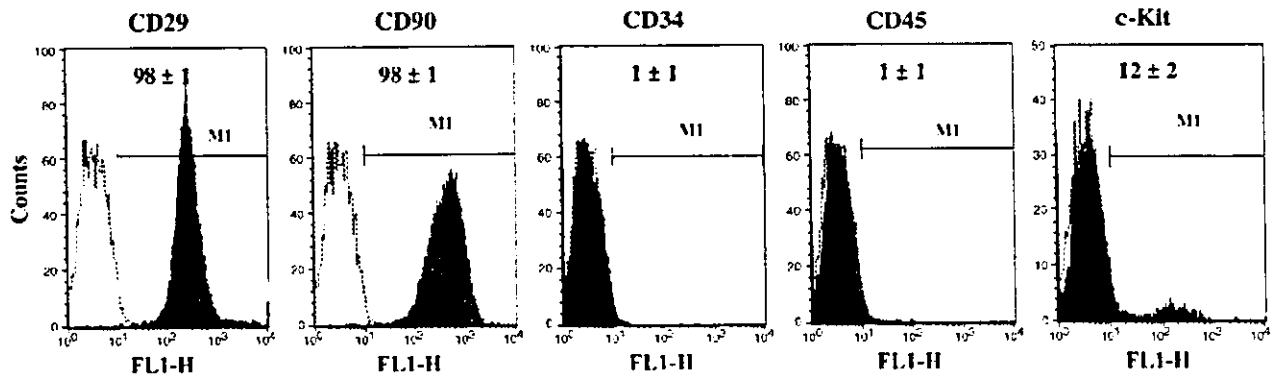

Fig. 1. Flow cytometric analysis of adherent, spindle-shaped mesenchymal stem cell (MSC) population expanded to 4–5 passages. Most of the cells expressed CD29 and CD90 but were negative for CD34 and CD45. Some cells were positive for c-Kit. MI, myocardial infarction.

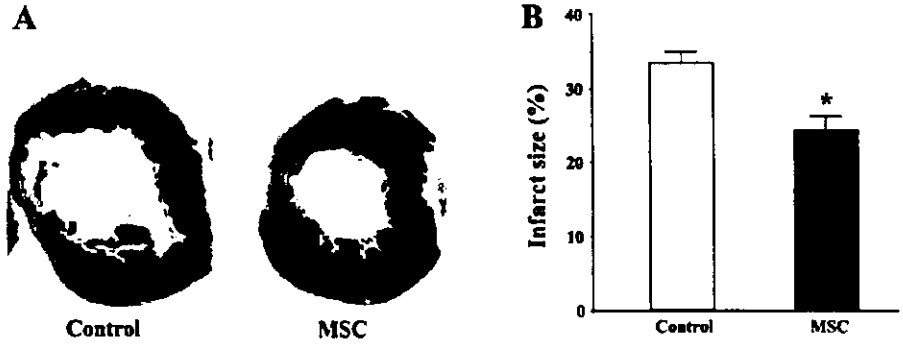

Fig. 2. Effect of MSC transplantation on myocardial infarct size 4 wk after myocardial infarction. *A*: representative Masson's trichrome-stained myocardial sections from control and MSC groups. *B*: quantitative analysis demonstrating that MSC transplantation significantly decreased infarct size. Values are means ± SE. $*P < 0.05$ vs. control.

transversely cut into 5-μm slices for calculation of the numbers of transplanted MSCs in the heart ($n = 5$).

Statistical analysis. Numerical values were expressed as means ± SE unless otherwise indicated. Comparisons of parameters among the three groups were made using one-way analysis of variance (ANOVA) followed by Scheffé's multiple comparison test. Comparisons of parameters between two groups were made by unpaired Student's *t*-test. $P < 0.05$ was considered significant.

RESULTS

Characterization of cultured MSCs. Most of cultured adherent cells expressed CD29 and CD90 (Fig. 1). In contrast, a majority of adherent cells were negative for CD34 and CD45. A small fraction of the adherent cells expressed c-Kit. Thus we confirmed that the major population of adherent cells was MSCs.

Reduction of myocardial infarct size after MSC transplantation. Moderate-to-large infarcts were observed in Masson's trichrome-stained myocardial sections 4 wk after coronary ligation (control group; Fig. 2*A*). However, MSC transplantation markedly decreased the infarct size after myocardial infarction (MSC group). Quantitative analysis also demonstrated that cardiac infarct size was significantly smaller in the MSC than in the control group: 24 ± 2 vs. 33 ± 2% ($n = 12$ each, $P < 0.05$; Fig. 2*B*).

Hemodynamic effects of MSC transplantation. At 4 wk after coronary ligation, hemodynamic studies were performed in the sham ($n = 11$), control ($n = 12$), and MSC ($n = 12$) groups. LV end-diastolic pressure showed a marked elevation in the control group (18 ± 1 mmHg); the elevation was significantly attenuated in the MSC group (13 ± 1 mmHg, $P < 0.05$; Fig. 3*A*). LV maximum dP/d*t* was significantly higher in the MSC than in the control group (Fig. 3*B*). LV minimum dP/d*t* tended to be lower in the MSC than in the control group (Fig. 3*C*). Although mean arterial pressure was significantly lower in the control than in the sham group, no decrease was observed in the MSC group (Table 1). Heart rate did not significantly differ among the three groups.

LV diastolic dimension was significantly smaller in the MSC than in the control group (Table 2). Fractional shortening was significantly greater in the MSC than in the control group (Fig. 3*D*). LV ejection fraction was also higher in the MSC than in

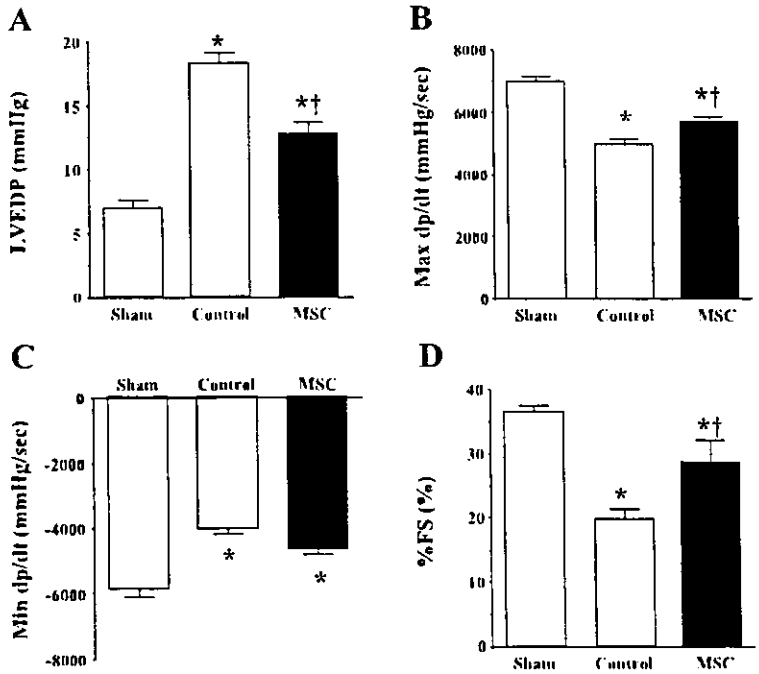

Fig. 3. Effects of MSC transplantation on hemodynamic parameters. LVEDP, LV end-diastolic pressure (*A*). max dP/d*t*, LV maximum dP/d*t* (*B*). Min dP/d*t*, LV minimum dP/d*t* (*C*). %FS, LV fractional shortening (*D*). Values are means ± SE. $*P < 0.05$ vs. sham. $†P < 0.05$ vs. control.

Table 1. *Characterization of animals*

	Sham (n = 11)	Control (n = 12)	MSC (n = 12)
Body wt, g	331 ± 4	301 ± 7*	321 ± 7†
LV wt/body wt, g/kg	1.83 ± 0.11	2.22 ± 0.10*	2.17 ± 0.09*
RV wt/body wt, g/kg	0.55 ± 0.02	0.83 ± 0.04*	0.71 ± 0.03*†
Heart rate, beats/min	404 ± 15	428 ± 17	418 ± 15
Mean arterial pressure, mmHg	128 ± 2	113 ± 4*	119 ± 3

Values are means ± SE. Sham, sham-operated rats given vehicle; control, myocardial infarction rats given vehicle; MSC, myocardial infarction rats given mesenchymal stem cells; LV, left ventricle; RV, right ventricle. *P < 0.05 vs. sham. †P < 0.05 vs. control.

Table 2. *Echocardiographic data*

	Sham	Control	MSC
LVD_d, mm	6.3 ± 0.1	8.6 ± 0.2*	7.5 ± 0.3*†
LVD_s, mm	4.0 ± 0.1	6.9 ± 0.3*	5.5 ± 0.5*†
%FS, %	37 ± 1	20 ± 2*	29 ± 3*†
LVEF, %	65 ± 1	39 ± 3*	53 ± 5*†
AWT diastole, mm	1.6 ± 0.1	1.1 ± 0.1*	1.4 ± 0.1†
PWT diastole, mm	1.6 ± 0.1	1.7 ± 0.1	1.7 ± 0.1

Values are means ± SE. LVD_d, LV diastolic dimension; LVD_s, LV systolic dimension; %FS, LV fractional shortening; LVEF, LV ejection fraction; AWT, anterior wall thickness; PWT, posterior wall thickness. *P < 0.05 vs. sham. †P < 0.05 vs. control.

the control group (Table 2). Diastolic anterior wall thickness was significantly attenuated in the MSC group compared with the control group.

Myogenesis and angiogenesis induced by MSCs. Red fluorescence-labeled MSCs were intravenously administered 3 h after coronary ligation (n = 5). Semiquantitative analysis demonstrated that ~3% of the transplanted MSCs were incorporated into the heart 24 h after transplantation. At 4 wk after transplantation (n = 5), MSCs were incorporated predominantly into the border zone of infarcts (Fig. 4), whereas few MSCs were detected in the noninfarcted myocardium. Immunofluorescence analyses demonstrated that the engrafted MSCs were positive for desmin (Fig. 4), cardiac troponin T (Fig. 5*A*), and connexin43 (Fig. 5*B*). These results suggest the ability of MSCs to engraft in the ischemic myocardium and differentiate into cardiomyocytes. On the other hand, some of the transplanted MSCs were positive for von Willebrand factor and formed vascular structures (Fig. 6). Alkaline phosphatase staining of the ischemic myocardium showed marked augmentation of neovascularization in the MSC group (Fig. 7*A*). Quantitative analysis demonstrated that capillary density was significantly higher in the MSC than in the control group (n = 5 each; Fig. 7*B*).

DISCUSSION

In the present study, we demonstrated that intravenously administered MSCs were capable of engraftment in the ischemic myocardium and that the engrafted MSCs differentiated into cardiomyocytes and vascular endothelial cells, resulting in myogenesis and angiogenesis. We also demonstrated that MSC transplantation decreased myocardial infarct size and improved cardiac function after acute myocardial infarction in rats.

Earlier studies showed that MSCs directly injected into the myocardium or those injected into coronary arteries improve cardiac function after myocardial infarction. However, little information is available regarding the therapeutic potential of systemically delivered MSCs for myocardial infarction. This study demonstrated that intravenous administration of MSCs

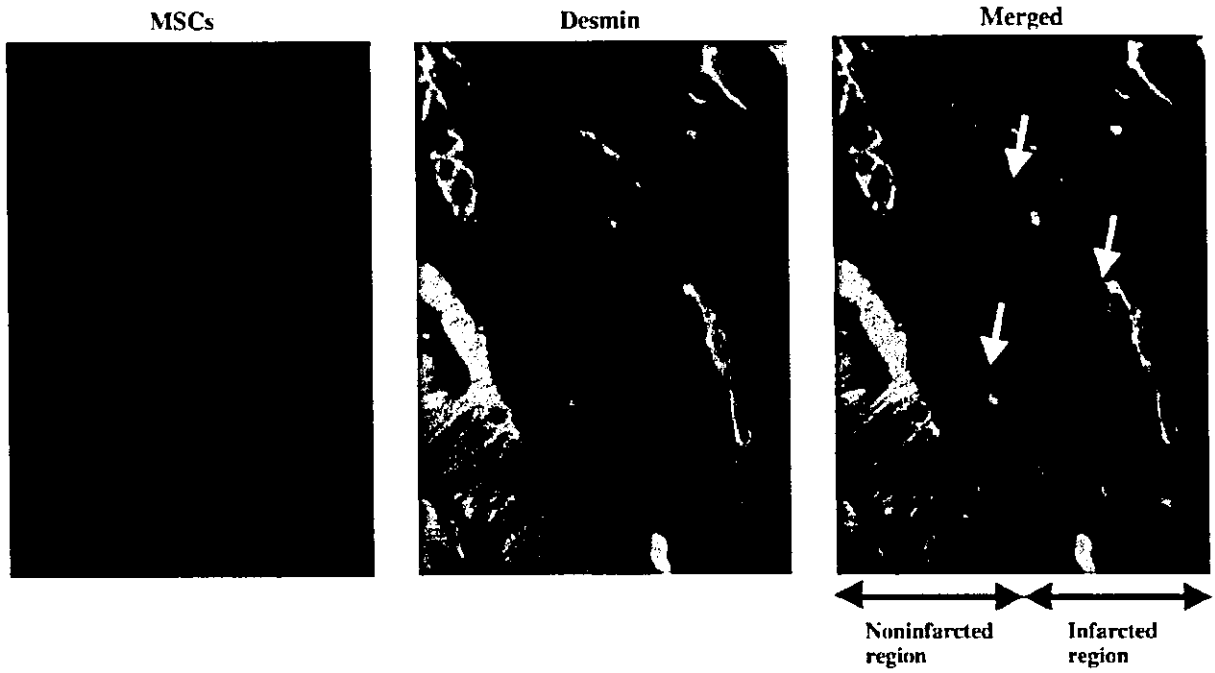

Fig. 4. Distribution of intravenously administered MSCs in myocardium after acute myocardial infarction. Red fluorescence-labeled MSCs were incorporated into ischemic boundary zone of the heart. These cells were positive for desmin (arrows), a cardiac marker. Magnification ×400.

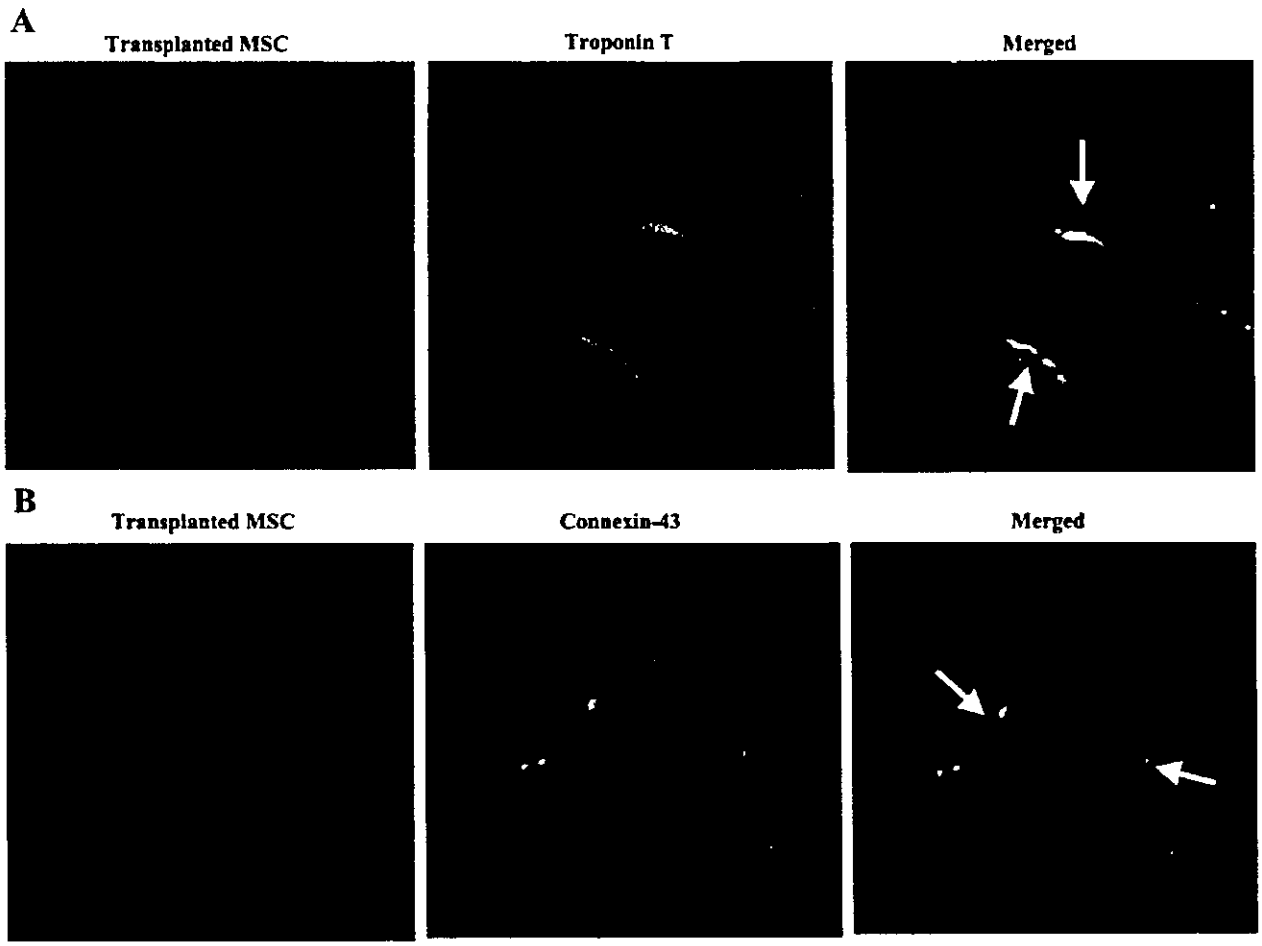

Fig. 5. Differentiation of transplanted MSCs in ischemic myocardium. Engrafted MSCs were positive (arrows) for cardiac troponin T (*A*) and connexin43 (*B*). Magnification ×400.

improves cardiac function after acute myocardial infarction through enhancement of angiogenesis and myogenesis in the ischemic myocardium.

Earlier studies showed that endothelial progenitor cells are mobilized from bone marrow into the peripheral blood in response to tissue ischemia and home to and incorporate into sites of neovascularization (21). Similar to epithelial progenitor cells, in the present study, transplanted MSCs were preferentially attracted to and retained in the border zone of infarcts. This is consistent with recent findings in the ischemic heart (5)

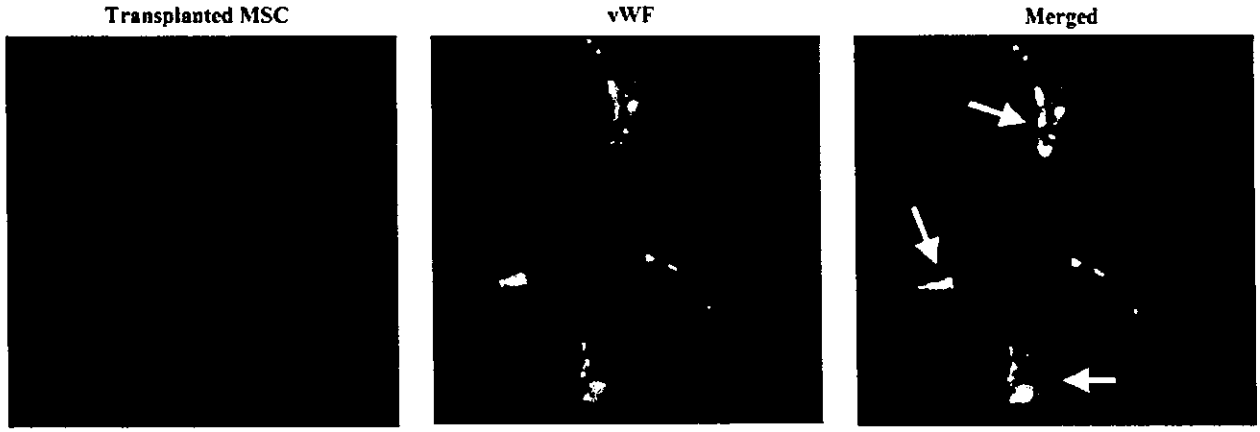

Fig. 6. Transplanted MSCs were positive for von Willebrand factor (vWF) and formed vascular structures. Magnification ×400.

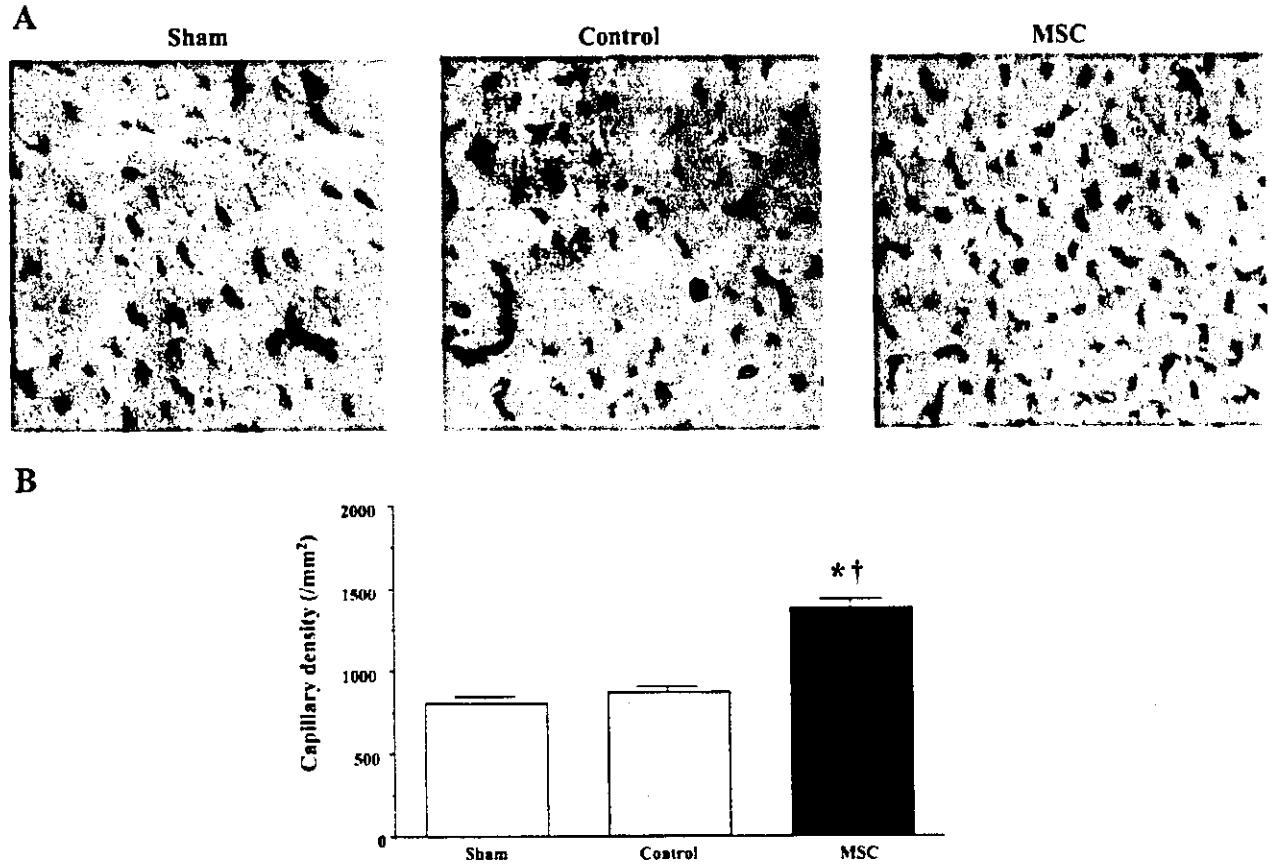

Fig. 7. *A*: representative samples of alkaline phosphatase staining in peri-infarct area. Magnification ×200. *B*: quantitative analysis of capillary density in peri-infarct area. Values are means ± SE. *$P < 0.05$ vs. sham. †$P < 0.05$ vs. control.

or brain (7). Although the underlying mechanisms remain unclear, ischemic tissue may express specific receptors or ligands to facilitate trafficking, adhesion, and infiltration of MSCs to ischemic sites.

In the present study, some of the engrafted MSCs were stained by cardiac proteins such as desmin and cardiac troponin T. Transplanted MSCs also expressed connexin43, a gap junction protein, at contact points with native cardiomyocytes. These results suggest that MSCs differentiated into cardiomyocytes in the ischemic myocardium and formed connections with native cardiomyocytes. In contrast to skeletal myoblasts, which have been used as a tool for myocardial repair, MSCs may have the capacity for electromechanical coupling. Earlier studies demonstrated the importance of the microenvironment for cardiomyogenic differentiation. Possible factors might include direct cell-cell contact (9), electrical and mechanical stimulation (10), and unknown growth factors. On the other hand, recent studies showed that stem cells may fuse with existing native cells (22, 25). Although the mechanisms by which MSCs develop into cardiomyocyte-like cells remain unclear, it is possible that the direct attachment with host cardiomyocytes in the ischemic myocardium contributes to the cardiogenic differentiation of transplanted MSCs. Further studies are necessary to investigate whether engrafted MSCs are actually becoming contractile.

In the present study, some of the transplanted MSCs were positive for an endothelial cell marker and participated in vessel formation. MSC transplantation significantly increased the capillary density in ischemic myocardium. The recently reported phenotypic plasticity of MSCs to transform into endothelial-like cells provides a rationale for their potential role in neovascularization. Hypoxia has been shown to induce MSC migration and capillary-like structure formation by upregulation of membrane type 1 matrix metalloproteinase (3). MSC implantation has been shown to induce therapeutic angiogenesis in a rat model of chronic hindlimb ischemia (1). These findings support the theory that intravenously administered MSCs are able to differentiate into vascular endothelial cells in the ischemic myocardium. Interestingly, MSCs enhance angiogenesis partly by increasing endogenous levels of vascular endothelial growth factor and vascular endothelial growth factor type 2 receptor (7). Together, these findings suggest that MSCs may contribute to neovascularization in the ischemic myocardium not only through their ability to generate capillary-like structures and but also through growth factor-mediated paracrine regulation.

The present study showed that MSC transplantation significantly reduced infarct size and attenuated wall thinning after acute myocardial infarction. Cardiomyocyte apoptosis during ischemia is one of the major contributors to the development of myocardial infarcts (16, 20). It is possible that newly formed vessels after MSC transplantation improve tissue perfusion around the ischemic boundary zone, resulting in functional recovery after acute myocardial infarction. We also demonstrated that transplanted

MSCs differentiated into cardiomyocytes in the ischemic myocardium. These results suggest that the decrease in infarct size and the increase in wall thickness may be attributable not only to MSC-induced neovascularization but also to myocardial regeneration. In the present study, MSC transplantation improved cardiac function after acute myocardial infarction, as indicated by a significant decrease in LV end-diastolic pressure, a tendency for an increase in maximum LV dP/dt, and a decrease in minimum LV dP/dt. Thus MSC-induced angiogenesis and myogenesis and the resultant reduced infarct size may have contributed to the hemodynamic improvement after acute myocardial infarction.

The low percentage of MSC migration to the heart is in agreement with some previous studies (5, 14). The present study also showed that only a small percentage of transplanted MSCs were incorporated into the heart. This may be explained by MSC apoptosis (12), tracking in the lung (5), and a dilution of the fluorescent dyes as the cells reproduce. Nevertheless, when MSCs were intravenously administered in an acute phase of myocardial infarction, MSCs induced angiogenesis and myogenesis and modestly, but significantly, improved cardiac function. Thus systemic delivery of MSCs may be beneficial for the treatment of myocardial infarction.

A limitation of this study is that the cell population may be mixed, rather than limited to MSCs, although cell surface markers of cultured cells were consistent with those of previously reported MSCs (12, 18).

In conclusion, intravenously administered MSCs were preferentially attracted to the infarcted myocardium and differentiated into vascular endothelial cells and cardiomyocytes. MSC transplantation decreased the infarct size and improved cardiac function after acute myocardial infarction through enhancement of angiogenesis and myogenesis. Thus MSC transplantation may be a new therapeutic strategy for the treatment of myocardial infarction.

GRANTS

This work was supported by Ministry of Health, Labour, and Welfare Cardiovascular Disease Research Grant 16C-6, the New Energy and Industrial Technology Development Organization of Japan Industrial Technology Research Grant Program in '03, Health and Labor Sciences Research Grants-genome 005, and Promotion of Fundamental Studies in Health Science of the Organization for Pharmaceutical Safety and Research of Japan

REFERENCES

1. **Al-Khaldi A, Al-Sabti H, Galipeau J, and Lachapelle K.** Therapeutic angiogenesis using autologous bone marrow stromal cells: improved blood flow in a chronic limb ischemia model. *Ann Thorac Surg* 75: 204–209, 2003.
2. **Al-Khaldi A, Eliopoulos N, Martineau D, Lejeune L, Lachapelle K, and Galipeau J.** Postnatal bone marrow stromal cells elicit a potent VEGF-dependent neoangiogenic response in vivo. *Gene Ther* 10: 621–629, 2003.
3. **Annabi B, Lee YT, Turcotte S, Naud E, Desrosiers RR, Champagne M, Eliopoulos N, Galipeau J, and Beliveau R.** Hypoxia promotes murine bone-marrow-derived stromal cell migration and tube formation. *Stem Cells* 21: 337–347, 2003.
4. **Asahara T, Murohara T, Sullivan A, Silver M, van der Zee R, Li T, Witzenbichler B, Schatteman G, and Isner JM.** Isolation of putative progenitor endothelial cells for angiogenesis. *Science* 275: 964–967, 1997.
5. **Barbash IM, Chouraqui P, Baron J, Feinberg MS, Etzion S, Tessone A, Miller L, Guetta E, Zipori D, Kedes LH, Kloner RA, and Leor J.** Systemic delivery of bone marrow-derived mesenchymal stem cells to the infarcted myocardium: feasibility, cell migration, and body distribution. *Circulation* 108: 863–868, 2003.
6. **Beltrami AP, Urbanek K, Kajstura J, Yan SM, Finato N, Bussani R, Nadal-Ginard B, Silvestri F, Leri A, Beltrami CA, and Anversa P.** Evidence that human cardiac myocytes divide after myocardial infarction. *N Engl J Med* 344: 1750–1757, 2001.
7. **Chen J, Zhang ZG, Li Y, Wang L, Xu YX, Gautam SC, Lu M, Zhu Z, and Chopp M.** Intravenous administration of human bone marrow stromal cells induces angiogenesis in the ischemic boundary zone after stroke in rats. *Circ Res* 92: 692–699, 2003.
8. **Chien YW, Barbee RW, MacPhee AA, Frohlich ED, and Trippodo NC.** Increased ANF secretion after volume expansion is preserved in rats with heart failure. *Am J Physiol Regul Integr Comp Physiol* 254: R185–R191, 1988.
9. **Fukuhara S, Tomita S, Yamashiro S, Morisaki T, Yutani C, Kitamura S, and Nakatani T.** Direct cell-cell interaction of cardiomyocytes is key for bone marrow stromal cells to go into cardiac lineage in vitro. *J Thorac Cardiovasc Surg* 125: 1470–1480, 2003.
10. **Iijima Y, Nagai T, Mizukami M, Matsuura K, Ogura T, Wada H, Toko H, Akazawa H, Takano H, Nakaya H, and Komuro I.** Beating is necessary for transdifferentiation of skeletal muscle-derived cells into cardiomyocytes. *FASEB J* 17: 1361–1363, 2003.
11. **Makino S, Fukuda K, Miyoshi S, Konishi F, Kodama H, Pan J, Sano M, Takahashi T, Hori S, Abe H, Hata J, Umezawa A, and Ogawa S.** Cardiomyocytes can be generated from marrow stromal cells in vitro. *J Clin Invest* 103: 697–705, 1999.
12. **Mangi AA, Noiseux N, Kong D, He H, Rezvani M, Ingwall JS, and Dzau VJ.** Mesenchymal stem cells modified with Akt prevent remodeling and restore performance of infarcted hearts. *Nat Med* 9: 1195–1201, 2003.
13. **Messina LM, Podrazik RM, Whitehill TA, Ekhterae D, Brothers TE, Wilson JM, Burkel WE, and Stanley JC.** Adhesion and incorporation of lacZ-transduced endothelial cells into the intact capillary wall in the rat. *Proc Natl Acad Sci USA* 89: 12018–12022, 1992.
14. **Muller P, Pfeiffer P, Koglin J, Schafers HJ, Seeland U, Janzen I, Urbschat S, and Bohm M.** Cardiomyocytes of noncardiac origin in myocardial biopsies of human transplanted hearts. *Circulation* 106: 31–35, 2002.
15. **Nagaya N, Nishikimi T, Yoshihara F, Horio T, Morimoto A, and Kangawa K.** Cardiac adrenomedullin gene expression and peptide accumulation after acute myocardial infarction in rats. *Am J Physiol Regul Integr Comp Physiol* 278: R1019–R1026, 2000.
16. **Narula J, Haider N, Virmani R, DiSalvo TG, Kolodgie FD, Hajjar RJ, Schmidt U, Semigran MJ, Dec GW, and Khaw BA.** Apoptosis in myocytes in end-stage heart failure. *N Engl J Med* 335: 1182–1189, 1996.
17. **Oh H, Bradfute SB, Gallardo TD, Nakamura T, Gaussin V, Mishina Y, Pocius J, Michael LH, Behringer RR, Garry DJ, Entman ML, and Schneider MD.** Cardiac progenitor cells from adult myocardium: homing, differentiation, and fusion after infarction. *Proc Natl Acad Sci USA* 100: 12313–12318, 2003.
18. **Pittenger MF, Mackay AM, Beck SC, Jaiswal RK, Douglas R, Mosca JD, Moorman MA, Simonetti DW, Craig S, and Marshak DR.** Multilineage potential of adult human mesenchymal stem cells. *Science* 284: 143–147, 1999.
19. **Reyes M, Dudek A, Jahagirdar B, Koodie L, Marker PH, and Verfaillie CM.** Origin of endothelial progenitors in human postnatal bone marrow. *J Clin Invest* 109: 337–346, 2002.
20. **Saraste A, Pulkki K, Kallajoki M, Henriksen K, Parvinen M, and Voipio-Pulkki LM.** Apoptosis in human acute myocardial infarction. *Circulation* 95: 320–323, 1997.
21. **Shake JG, Gruber PJ, Baumgartner WA, Senechal G, Meyers J, Redmond JM, Pittenger MF, and Martin BJ.** Mesenchymal stem cell implantation in a swine myocardial infarct model: engraftment and functional effects. *Ann Thorac Surg* 73: 1919–1925, 2002.
22. **Terada N, Hamazaki T, Oka M, Hoki M, Mastalerz DM, Nakano Y, Meyer EM, Morel L, Petersen BE, and Scott EW.** Bone marrow cells adopt the phenotype of other cells by spontaneous cell fusion. *Nature* 416: 542–545, 2002.
23. **Toma C, Pittenger MF, Cahill KS, Byrne BJ, and Kessler PD.** Human mesenchymal stem cells differentiate to a cardiomyocyte phenotype in the adult murine heart. *Circulation* 105: 93–98, 2002.
24. **Wang JS, Shum-Tim D, Galipeau J, Chedrawy E, Eliopoulos N, and Chiu RC.** Marrow stromal cells for cellular cardiomyoplasty: feasibility and potential clinical advantages. *J Thorac Cardiovasc Surg* 120: 999–1005, 2000.
25. **Ying QL, Nichols J, Evans EP, and Smith AG.** Changing potency by spontaneous fusion. *Nature* 416: 545–548, 2002.

Demonstration of enhanced *K*-edge angiography using a cerium target x-ray generator

Eiichi Sato[a)]
Department of Physics, Iwate Medical University, Morioka 020-0015, Japan

Etsuro Tanaka
Department of Nutritional Science, Faculty of Applied Bio-science, Tokyo University of Agriculture, Setagayaku 156-8502, Japan

Hidezo Mori
Department of Cardiac Physiology, National Cardiovascular Center Research Institute, Osaka 565-8565, Japan

Toshiaki Kawai
Electron Tube Division #2, Hamamatsu Photonics Inc., Iwata-gun 438-0193, Japan

Toshio Ichimaru
Department of Radiological Technology, School of Health Sciences, Hirosaki University, Hirosaki 036-8564, Japan

Shigehiro Sato
Department of Microbiology, School of Medicine, Iwate Medical University, Morioka 020-8505, Japan

Kazuyoshi Takayama
Shock Wave Research Center, Institute of Fluid Science, Tohoku University, Sendai 980-8577, Japan

Hideaki Ido
Department of Applied Physics and Informatics, Faculty of Engineering, Tohoku Gakuin University, Tagajo 985-8537, Japan

(Received 18 May 2004; revised 8 July 2004; accepted for publication 14 August 2004; published 22 October 2004)

The cerium target x-ray generator is useful in order to perform enhanced *K*-edge angiography using a cone beam because *K*-series characteristic x rays from the cerium target are absorbed effectively by iodine-based contrast mediums. The x-ray generator consists of a main controller, a unit with a Cockcroft-Walton circuit and a fixed anode x-ray tube, and a personal computer. The tube is a glass-enclosed diode with a cerium target and a 0.5-mm-thick beryllium window. The maximum tube voltage and current were 65 kV and 0.4 mA, respectively, and the focal-spot sizes were 1.0 $\times$1.3 mm. Cerium $K\alpha$ lines were left using a barium sulfate filter, and the x-ray intensity was 0.48 μC/kg at 1.0 m from the source with a tube voltage of 60 kV, a current of 0.40 mA, and an exposure time of 1.0 s. Angiography was performed with a computed radiography system using iodine-based microspheres. In coronary angiography of nonliving animals, we observed fine blood vessels of approximately 100 μm with high contrasts. © *2004 American Association of Physicists in Medicine.* [DOI: 10.1118/1.1803433]

Key words: x-ray source, x-ray tube, x-ray spectra, attenuation coefficient, angiography

I. INTRODUCTION

Synchrotrons generate monochromatic parallel x-ray beams using single crystals. These beams with photon energies of approximately 35 keV have been employed to perform enhanced *K*-edge angiography,[1–4] since the beams are absorbed effectively by iodine-based contrast mediums. However, it is difficult to increase the irradiation field, due to the parallel beam, and to obtain sufficient machine times for various research projects, including medical applications.

Currently, flash x-ray generators utilize cold-cathode radiation tubes and produce extremely short x-ray pulses of less than 1 μs. So far, several different flash x-ray generators have been developed,[5] and the generators with photon energies of lower than 150 keV[6–11] can be employed to perform biomedical radiography. In order to produce monochromatic x rays, plasma flash x-ray generators are useful, since quite intense and clean characteristic x rays have been produced from weakly ionized linear plasmas of nickel, copper,[12] and molybdenum,[13] while bremsstrahlung rays are hardly detected at all. Using these generators, the characteristic x-ray intensity substantially increased with corresponding increases in the charging voltage.

Since *K*-series characteristic x rays from cerium target are absorbed effectively by iodine-based contrast mediums, a cerium-target x-ray tube is very useful in order to perform high contrast angiography. On the other hand, cerium is a rare earth element and has a high reactivity, and it is difficult to design the target. However, we are very interested in pro-

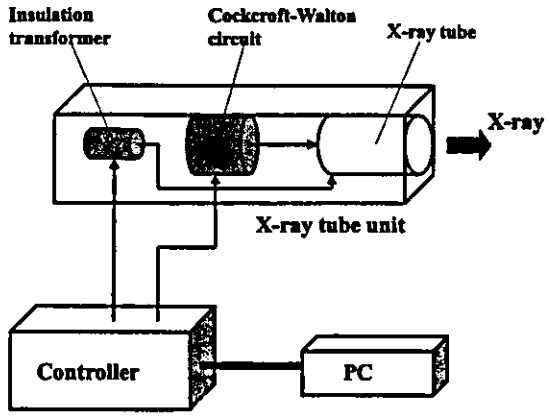

FIG. 1. Block diagram of the compact x-ray generator with a cerium-target radiation tube, which is used specially for *K*-edge angiography using iodine-based contrast mediums.

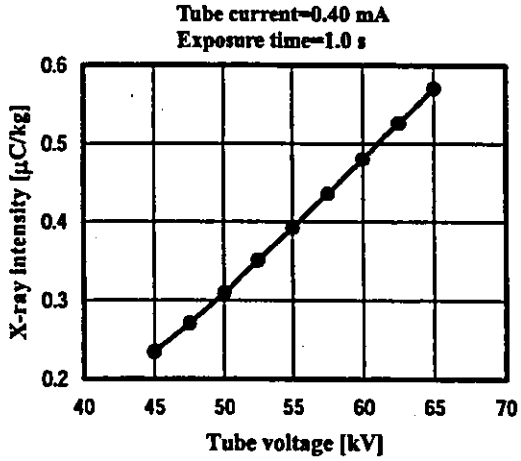

FIG. 3. X-ray intensity measured at 1.0 m from the x-ray source according to changes in the tube voltage.

ducing cerium characteristic x rays to perform cone beam angiography because the irradiation field can be increased easily.

In the present research, we developed a compact x-ray generator with a cerium target tube, and used it to perform a preliminary study on enhanced *K*-edge angiography achieved with cerium $K\alpha$ rays.

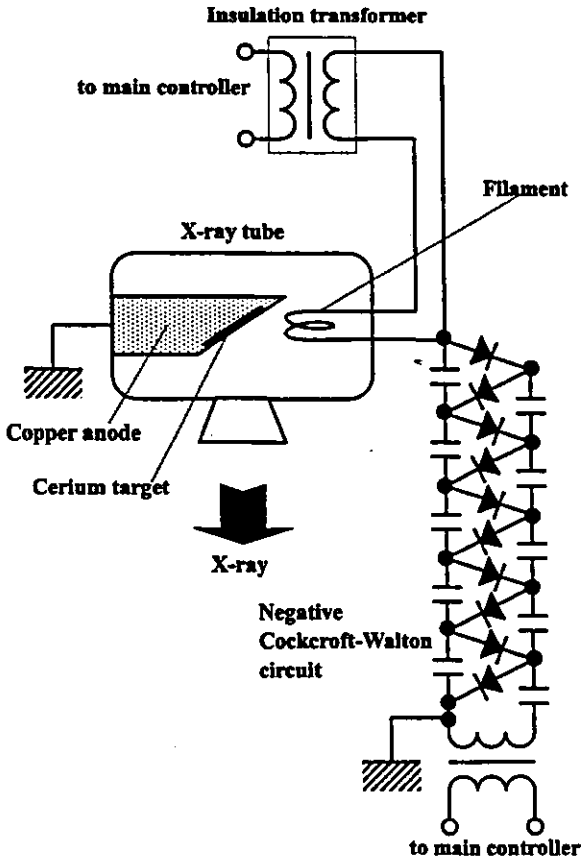

FIG. 2. Main circuit of the x-ray generator.

II. GENERATOR

Figure 1 shows the block diagram of the x-ray generator, which consists of a main controller, an x-ray tube unit with a Cockcroft-Walton circuit, and a cerium-target tube, and a personal computer. The tube voltage, the current, and the exposure time can be controlled by both the controller and the computer. The main circuit for producing x rays is illustrated in Fig. 2, and employed the Cockcroft-Walton circuit in order to decrease the dimensions of the tube unit. In the circuit, the condensers are always in series, and are charged serially. In the x-ray tube, the negative high voltage is applied to the cathode electrode, and the anode (target) is connected to the tube unit case (ground potential) to cool the anode and the target effectively. The filament heating current is supplied by an ac power supply in the controller in conjunction with an insulation transformer which is used for isolation from the high voltage from the Cockcroft-Walton circuit. In this experiment, the tube voltage applied was from 45 to 65 kV, and the tube current was regulated to within 0.40 mA (maximum current) by the filament temperature. The exposure time is controlled in order to obtain optimum x-ray intensity. Monochromatic $K\alpha$ lines were left using a 5-mm-thick barium sulfate filter in which barium sulfate powder was mixed with polymethyl methacrylate (PMMA) resin, since both the bremsstrahlung and the $K\beta$ rays were absorbed effectively by the filter. In designing the filter, the surface density of the barium sulfate powder is important, since the x rays are absorbed effectively by the powder as compared with the PMMA resin. In this case, the density was 7.6 mg/cm^2.

III. CHARACTERISTICS

A. X-ray intensity

X-ray intensity was measured by a Victoreen 660 ionization chamber at 1.0 m from the x-ray source using the filter with an exposure time of 1.0 s (Fig. 3). At a constant tube current of 0.40 mA, the x-ray intensity increased when the tube voltage was increased. In this measurement, the inten-

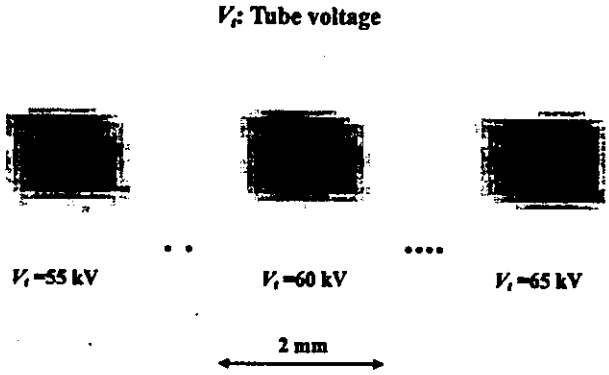

FIG. 4. Effective focal spots with changes in the tube voltage.

sity with a tube voltage of 60 kV and a current of 0.40 mA was 0.48 μC/kg at 1.0 m from the source with errors of less than 0.2%.

B. Focal spot

In order to measure images of the x-ray source after the barium sulfate filtration, we employed a pinhole camera with a hole diameter of 50 μm (magnification ratio of 1:1) in conjunction with a computed radiography (CR) system[14,15] with a sampling pitch of 87.5 μm. When the tube voltage was increased, spot dimensions seldom varied and had values of 1.0×1.3 mm (Fig. 4).

C. X-ray spectra

In order to measure x-ray spectra, we employed a cadmium tellurium detector (CDTE2020X, Hamamatsu Photonics Inc.) (Fig. 5). Compared with a germanium detector, this detector has a lower energy resolution of 1.7 keV. When the tube voltage was increased, the characteristic x-ray intensities of $K\alpha$ lines increased, and both the maximum photon energy and the intensities of bremsstrahlung x rays increased. The barium sulfate filter significantly attenuate the spectra above the barium K-edge energy of 37.399 keV. The areas under the spectral curves correlate closely to the total x-ray intensities shown in Fig. 3.

IV. ANGIOGRAPHY

Figure 6 shows the mass attenuation coefficients of iodine at the selected energies; the coefficient curve is discontinuous at the iodine K edge. The average photon energy of the cerium $K\alpha$ lines is shown just above the iodine K edge. Cerium is a rare earth element and has a high reactivity; however, the average photon energy of $K\alpha$ lines is 34.566 keV, and iodine contrast mediums with a K-absorption edge of 33.155 keV absorb the lines easily. Therefore, blood vessels were observed with high contrasts. Subsequently, in angiography testing, we usually employ nonliving animal phantoms using microspheres.

The angiography was performed by the CR system (Konica Regius 150) using the filter, and the distance (between the x-ray source and the imaging plate) was 1.5 m.

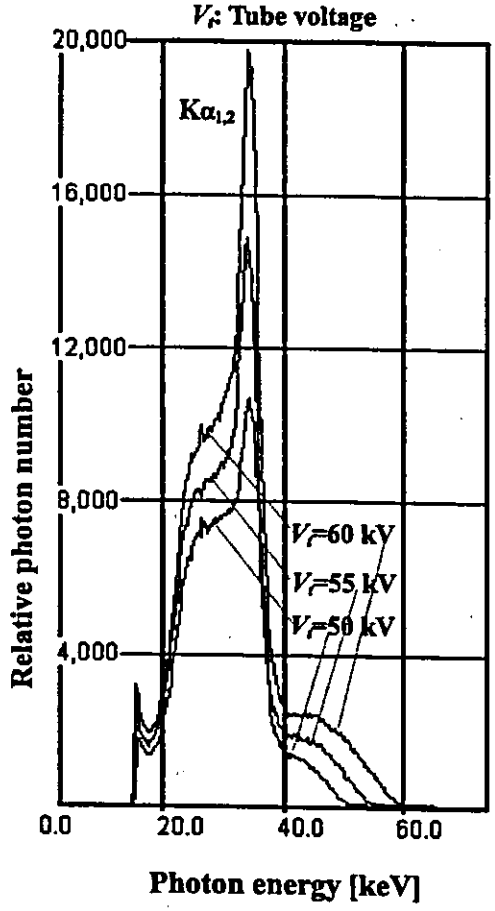

FIG. 5. X-ray spectra measured by a cadmium tellurium detector with changes in the tube voltage.

First, rough measurements of image resolution were made using wires. Figure 7 shows radiograms of tungsten wires in a rod made of PMMA with a tube voltage of 60 kV. Although the image contrast decreased somewhat with decreases in the wire diameter, due to blurring of the image caused by the sampling pitch of 87.5 μm, a 50-μm-diameter wire could be observed.

Angiograms of rabbit hearts are shown in Fig. 8. These two images were obtained using iodine and cerium micro-

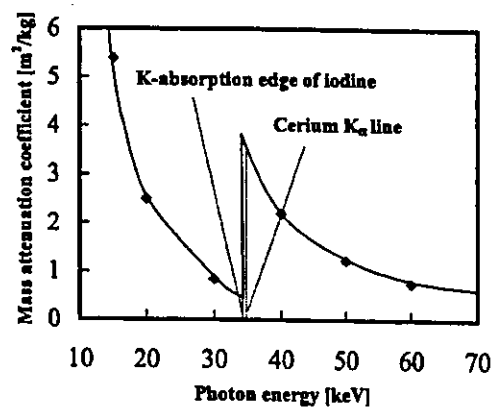

FIG. 6. Mass attenuation coefficients of iodine, and the average photon energy of the cerium $K\alpha$ lines is shown just above the iodine K edge.

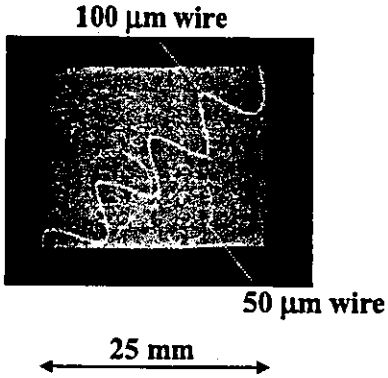

FIG. 7. Radiograms of tungsten wires in a PMMA rod with a tube voltage of 60 kV.

spheres of 15 μm in diameter at a tube voltage of 60 kV. The iodine spheres contained 37% iodine by weight, and the cerium spheres contained 18% cerium by weight. The concentration of spheres in the blood varies with the filling rate, and the estimated densities of the iodine and the cerium of blood are less than 0.44 and 0.17 g/cm^3, respectively. In the case where the cerium spheres were employed, the coronary arteries were barely visible. Figure 9(a) shows an angiogram of a larger dog heart using the cerium target at a tube voltage of 60 kV using iodine spheres. For comparison, we performed angiography with a tungsten x-ray tube at a tube voltage of 60 kV [Fig. 9(b)].

If we assume that the filling rate of the iodine microspheres in a blood vessel is constant, the image contrast of the blood is in inverse proportion to the vessel diameter. Next, the density ratios (maximum density divided by minimum density) obtained by the cerium and tungsten tubes were 4.3 and 2.7, respectively. In angiography using the tungsten target, blood vessels of approximately 100 μm were hardly observed at all.

V. DISCUSSION

In summary, we developed a x-ray generator with a cerium-target tube and succeeded in producing cerium $K\alpha$ lines, which can be absorbed easily by iodine-based contrast mediums. Both the characteristic and bremsstrahlung x-ray intensities increased with increases in the tube voltage, and $K\beta$ lines were absorbed effectively by the barium sulfate filter. The x-ray intensity was limited because the thermal contact between the target and the anode was not good. However, the intensity can be increased by welding the target or using a cerium-alloy target.

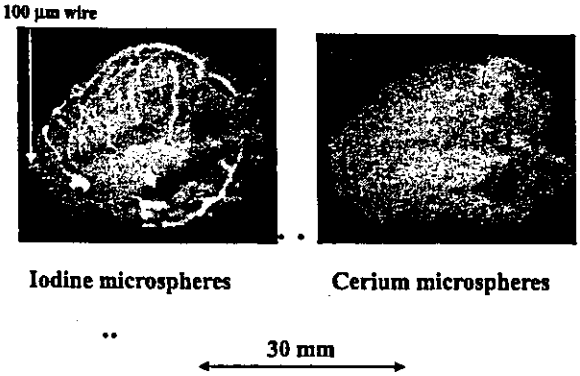

FIG. 8. Angiograms of extracted rabbit hearts using iodine and cerium microspheres with a tube voltage of 60 kV.

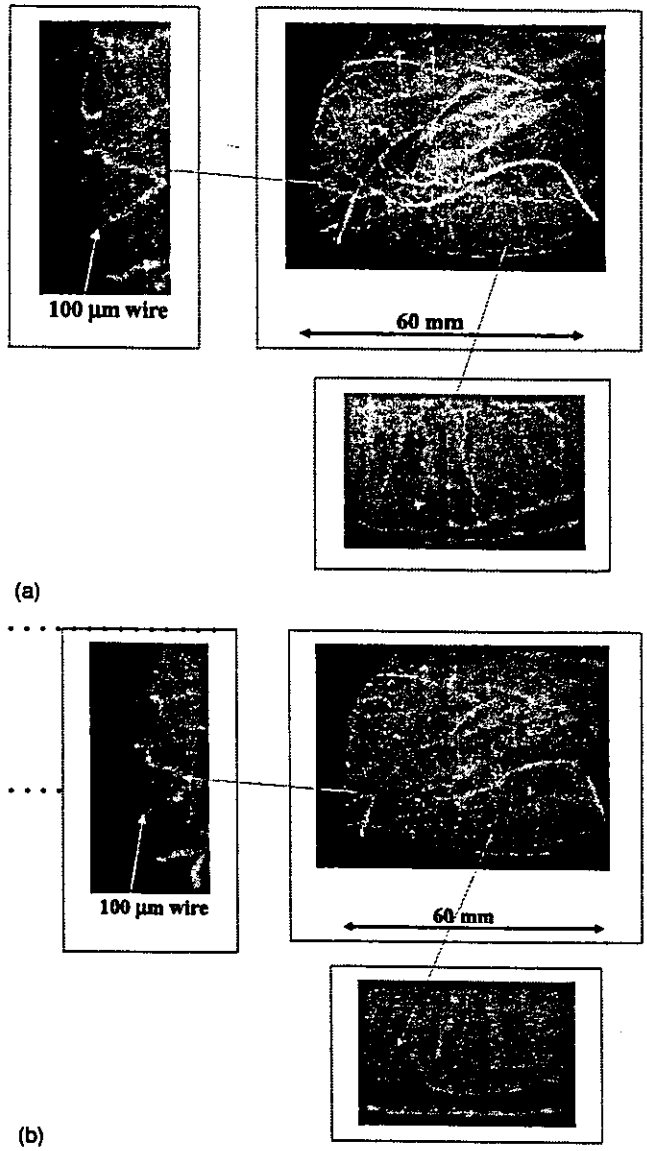

FIG. 9. Angiograms of an extracted dog heart achieved with (a) cerium and (b) tungsten target x-ray tubes using iodine microspheres with a tube voltage of 60 kV.

In this preliminary experiment, although the maximum tube voltage and current were 65 kV and 0.40 mA, respectively, the voltage and current could be increased. Subsequently, the generator produced maximum number of characteristic photons was approximately 3×10^7 photons/cm^2 s at 1.0 m from the source, and the photon count rate can be increased easily by improving the target.

Since the sampling pitch of the CR system is 87.5 μm, we obtained resolutions of approximately 100 μm, and high-contrast blood vessels could be observed using a CR system. In order to observe fine blood vessels of less than 100 μm,

the image resolution of the CR system should be improved as much as possible, and a flat panel system is useful to observe blood flows for cases of cardiovascular disease.

ACKNOWLEDGMENTS

This work was supported by Grants-in-Aid for Scientific Research and Advanced Medical Scientific Research from MECSST (13470154, 13877114, and 16591222), Grants from Keiryo Research Foundation, JST (Test of Fostering Potential), NEDO, and MHLW (HLSRG, RAMT-nano-001, RHGTEFB-genome-005, and RGCD13C-1).

[a]Author to whom correspondence should be addressed. Department of Physics, Iwate Medical University, 3-16-1 Honchodori, Morioka 020-0015, Japan; electronic mail: dresato@iwate-med.ac.jp

[1]A. Akisada, M. Ando, K. Hyodo, S. Hasegawa, K. Konishi, K. Nishimura, A. Maruhashi, F. Toyofuku, A. Suwa, and K. Kohra, "An attempt at coronary angiography with a large size monochromatic SR beam," Nucl. Instrum. Methods Phys. Res. A **246**, 713–718 (1986).

[2]A. C. Thompson, H. D. Zeman, G. S. Brown, J. Morrison, P. Reiser, V. Padmanabahn, L. Ong, S. Green, J. Giacomini, H. Gordon, and E. Rubenstein, "First operation of the medical research facility at the NSLS for coronary angiography," Rev. Sci. Instrum. **63**, 625–628 (1992).

[3]H. Mori, K. Hyodo, E. Tanaka, M. U. Mohammed, A. Yamakawa, Y. Shinozaki, H. Nakazawa, Y. Tanaka, T. Sekka, Y. Iwata, S. Honda, K. Umetani, H. Ueki, T. Yokoyama, K. Tanioka, M. Kubota, H. Hosaka, N. Ishizawa, and M. Ando, "Small-vessel radiography in situ with monochromatic synchrotoron radiation," Radiology **201**, 173–177 (1996).

[4]K. Hyodo, M. Ando, Y. Oku, S. Yamamoto, T. Takeda, Y. Itai, S. Ohtsuka, Y. Sugishita, and J. Tada, "Development of a two-dimensional imaging system for clinical applications of intravenous coronary angiography using intense synchrotron radiation produced by a multipole wiggler," J. Synchrotron Radiat. **5**, 1123–1126 (1998).

[5]R. Germer, "X-ray flash techniques," J. Phys. E **12**, 336–350 (1979).

[6]E. Sato, H. Isobe, and F. Hoshino, "High intensity flash x-ray apparatus for biomedical radiography," Rev. Sci. Instrum. **57**, 1399–1408 (1986).

[7]E. Sato, S. Kimura, S. Kawasaki, H. Isobe, K. Takahashi, Y. Tamakawa, and T. Yanagisawa, "Repetitive flash x-ray generator utilizing a simple diode with a new type of energy-selective function," Rev. Sci. Instrum. **61**, 2343–2348 (1990).

[8]A. Shikoda, E. Sato, M. Sagae, T. Oizumi, Y. Tamakawa, and T. Yanagisawa, "Repetitive flash x-ray generator having a high-durability diode driven by a two-cable-type line pulser," Rev. Sci. Instrum. **65**, 850–856 (1994).

[9]E. Sato, K. Takahashi, M. Sagae, S. Kimura, T. Oizumi, Y. Hayasi, Y. Tamakawa, and T. Yanagisawa, "Sub-kilohertz flash x-ray generator utilizing a glass-enclosed cold-cathode triode," Med. Biol. Eng. Comput. **32**, 289–294 (1994).

[10]K. Takahashi, E. Sato, M. Sagae, T. Oizumi, Y. Tamakawa, and T. Yanagisawa, "Fundamental study on a long-duration flash x-ray generator with a surface-discharge triode," Jpn. J. Appl. Phys., Part 1 **33**, 4146–4151 (1994).

[11]E. Sato, M. Sagae, K. Takahashi, A. Shikoda, T. Oizumi, Y. Hayasi, Y. Tamakawa, and T. Yanagisawa, "10 kHz microsecond pulsed x-ray generator utilizing a hot-cathode triode with variable durations for biomedical radiography," Med. Biol. Eng. Comput. **32**, 295–301 (1994).

[12]E. Sato, Y. Hayasi, R. Germer, E. Tanaka, H. Mori, T. Kawai, T. Ichimaru, K. Takayama, and H. Ido, "Quasi-monochromatic flash x-ray generator utilizing weakly ionized linear copper plasma," Rev. Sci. Instrum. **74**, 5236–5240 (2003).

[13]E. Sato, Y. Hayasi, R. Germer, E. Tanaka, H. Mori, T. Kawai, H. Obara, T. Ichimaru, K. Takayama, and H. Ido, "Irradiation of intense characteristic x-rays from weakly ionized linear molybdenum plasma," Jpn. J. Med. Phys. **23**, 123–131 (2003).

[14]M. Sonoda, M. Takano, J. Miyahara, and H. Kato, "Computed radiography utilizing scanning laser stimulated luminescence," Radiology **148**, 833–838 (1983).

[15]E. Sato, K. Sato, and Y. Tamakawa, "Film-less computed radiography system for high-speed imaging," Ann. Rep. Iwate Med. Univ. Sch. Lib. Arts and Sci. **35**, 13–23 (2000).

Compact monochromatic flash x-ray generator utilizing a disk-cathode molybdenum tube

Eiichi Sato[a)]
Department of Physics, Iwate Medical University, 3-16-1 Honchodori Morioka 020-0015, Japan

Etsuro Tanaka
Department of Nutritional Science, Faculty of Applied Bio-science, Tokyo University of Agriculture, Setagayaku 156-8502, Japan

Hidezo Mori
Department of Cardiac Physiology, National Cardiovascular Center Research Institute, Osaka 565-8565 Japan

Toshiaki Kawai
Electron Tube Division #2, Hamamatsu Photonics K. K., Iwata-gun 438-0193, Japan

Toshio Ichimaru
Department of Radiological Technology, School of Health Sciences, Hirosaki University, Hirosaki 036-8564, Japan

Shigehiro Sato
Department of Microbiology, School of Medicine, Iwate Medical University, Morioka 020-8505, Japan

Kazuyoshi Takayama
Shock Wave Research Center, Institute of Fluid Science, Tohoku University, Sendai 980-8577, Japan

Hideaki Ido
Department of Applied Physics and Informatics, Faculty of Engineering, Tohoku Gakuin University, Tagajo 985-8537, Japan

(Received 8 April 2004; revised 16 October 2004; accepted for publication 18 October 2004; published 15 December 2004)

The high-voltage condensers in a polarity-inversion two-stage Marx surge generator are charged from −50 to −70 kV by a power supply, and the electric charges in the condensers are discharged to an x-ray tube after closing gap switches in the surge generator with a trigger device. The x-ray tube is a demountable diode, and the turbo molecular pump evacuates air from the tube with a pressure of approximately 1 mPa. Clean molybdenum Kα lines are produced using a 20 μm-thick zirconium filter, since the tube utilizes a disk cathode and a rod target, and bremsstrahlung rays are not emitted in the opposite direction to that of electron acceleration. At a charging voltage of −70 kV, the instantaneous tube voltage and current were 120 kV and 1.0 kA, respectively. The x-ray pulse widths were approximately 70 ns, and the generator produced instantaneous number of Kα photons was approximately 3×10^7 photons/cm^2 per pulse at 0.5 m from the source of 3.0 mm in diameter. © *2005 American Association of Physicists in Medicine.* [DOI: 10.1118/1.1829247]

Key words: x-ray source, x-ray tube, x-ray spectra, rapid imaging, x-ray beam filtration, monochromatic x ray

I. INTRODUCTION

In recent years, many valuable discoveries have been made in laser technology, and soft x-ray lasers of neonlike argon (46.9 nm, 26.4 eV) have been produced using a gas-discharge capillary.[1–3] In these experiments, the laser energy increased with increases in the capillary length, and these kinds of first discharges can generate hot and dense plasma columns with aspect ratios of 1000:1. However, it is difficult to increase the laser photon energy to 10 keV or beyond.

We have developed several different soft flash x-ray generators[4–8] corresponding to specific radiographic objectives, and a major goal in our research is the development of an intense and clean monochromatic x-ray generator that can impact applications with medical radiography. In view of this situation, we confirmed irradiation of intense K-series characteristic x rays from the plasma axial direction by forming weakly ionized linear plasma.[9–12] In the plasma, bremsstrahlung spectra with photon energies of higher than the K-absorption edge are effectively absorbed and are converted into fluorescent x rays, and the plasma then transmits the fluorescent rays easily. However, the bremsstrahlung x rays are produced using a molybdenum target,[11] since high photon energy bremsstrahlung x rays are not absorbed effectively in the linear plasma.

Without forming the linear plasma, because bremsstrahlung rays are not emitted in the opposite direction to that of electron acceleration, characteristic x rays can be produced by considering the angle dependence of bremsstrahlung x rays. As compared with the plasma generator, the photon

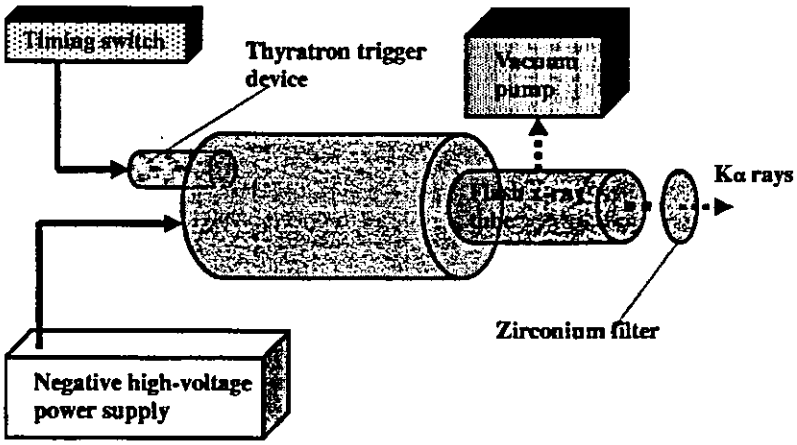

FIG. 1. Block diagram of the compact quasimonochromatic flash x-ray generator with a cold-cathode monochromatic diode.

energy of the characteristic x rays can be increased by increasing the maximum output voltage of the pulse generator, since a multistage Marx generator[13,14] can be employed. In this case, the output voltage is equal to the value of the condenser charging voltage multiplied by the stage number.

In this article, we describe a compact flash x-ray generator utilizing a molybdenum-target radiation tube, used to perform a preliminary experiment for producing clean monochromatic x rays.

II. GENERATOR

A. High-voltage circuit

Figure 1 shows a block diagram of a compact monochromatic flash x-ray generator. This generator consists of the following components: a constant high-voltage power supply, a surge Marx generator with a capacity during main discharge of 425 pF, a thyratron trigger device of the surge generator, a turbo molecular pump, and a flash x-ray tube. Since the electric circuit of the high-voltage pulse generator employs a polarity-inversion two-stage Marx line[13,14] (Fig. 2), the surge generator produces twice the potential of the condenser charging voltage. When two condensers inside of the surge generator are charged from −50 to −70 kV, the ideal output voltage ranges from 100 to 140 kV.

B. X-ray tube

The x-ray tube is a demountable diode type, as illustrated in Fig. 3. This tube is connected to the turbo molecular pump with a pressure of about 1 mPa and consists of the following major devices: a rod-shaped molybdenum target 3.0 mm in diameter, a disk cathode made of graphite, a polyethylene terephthalate (Mylar) x-ray window 0.25 mm in thickness, and a polymethyl methacrylate tube body. The target-cathode space was regulated to 1.0 mm from the outside of the x-ray tube by rotating the anode rod, and the transmission x rays are obtained through a 1.0 mm-thick graphite cathode and an x-ray window. Because bremsstrahlung rays are not emitted in the opposite direction to that of electron acceleration (Fig. 4), molybdenum Kα rays can be produced using a 20 μm-thick zirconium K-edge filter.

III. CHARACTERISTICS

A. Tube voltage and current

Tube voltage and current were measured by a high-voltage divider with an input impedance of 10 kΩ and a current transformer, respectively (Fig. 5). The voltage and current displayed roughly damped oscillations because the discharge resistance in the tube varied rapidly from infinity

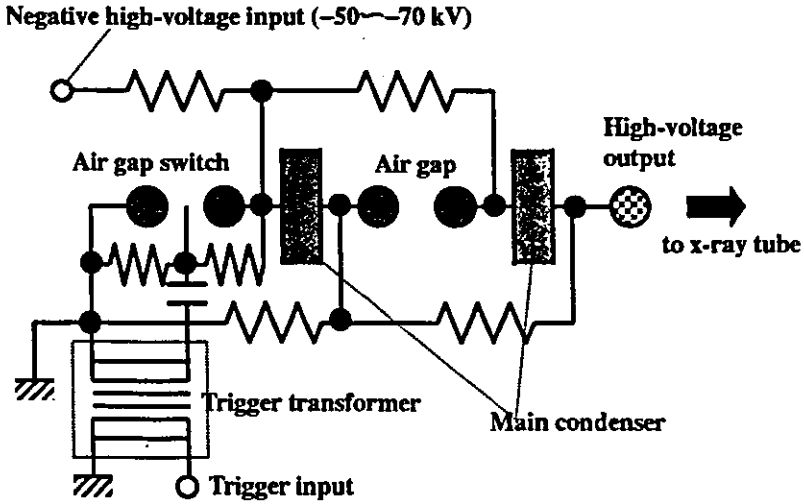

FIG. 2. Circuit diagram of the two-stage surge Marx generator. The generator produces twice the potential of the condenser charging voltage.

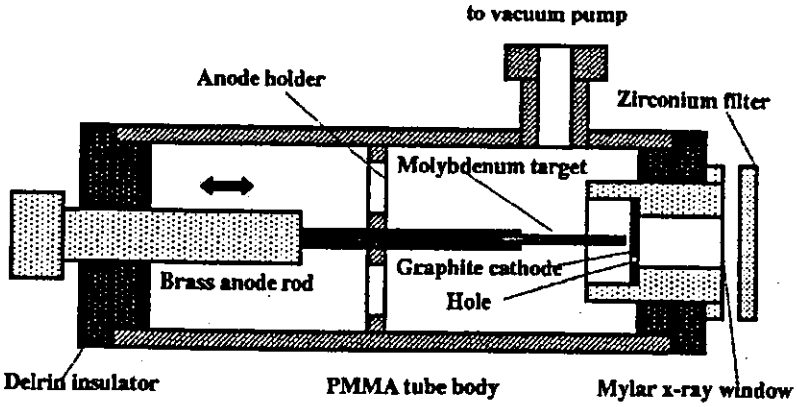

FIG. 3. Schematic drawing of the flash x-ray tube with a rod-shaped molybdenum target and a disk graphite cathode.

to approximately 0 Ω during the discharge. Thus, at the first quarter cycle of the oscillations, when the voltage decreased, the current increased. The instantaneous voltage and current increased with increases in the charging voltage, and the voltage and current were approximately 120 kV and 1.0 kA, respectively, at a charging voltage of −70 kV.

B. X-ray output

X-ray output pulse was detected using a combination of a plastic scintillator, a photomultiplier, and the filter (Fig. 6). When the charging voltage was increased, the pulse height increased, but the width seldom varied. The widths were about 70 ns, and the time-integrated x-ray dose measured by a thermoluminescence dosimeter (Kyokko TLD Reader 1500 having MSO-S elements without energy compensation) had an instantaneous value of approximately 70 μGy per pulse at 0.5 m from the x-ray source with a charging voltage of −70 kV.

C. X-ray source

In order to observe the Kα x-ray source, we employed a 100 μm-diameter pinhole camera, an x-ray film (Polaroid XR-7), and the filter (Fig. 7). When the charging voltage was increased, the spot intensity increased, and the intensities corresponded well to the x-ray pulse height. The dimension was almost equal to the target diameter and had a value of about 3.0 mm.

D. X-ray spectra

X-ray spectra were measured using a transmission-type spectrometer[11] with a lithium fluoride curved crystal 0.5 mm in thickness. The x-ray intensities of the spectra were detected by an imaging plate of a computed radiography (CR) system[15] (Konica Regius 150) with a wide dynamic range, and relative x-ray intensity was calculated from Dicom original digital data corresponding to x-ray intensity; the data was scanned by Dicom viewer in the film-less CR system. Subsequently, the relative x-ray intensity as a function of the data was calibrated using a conventional x-ray generator, and we confirmed that the intensity was proportional to the exposure time. Figure 8 shows measured spectra from the molybdenum target with the filter. In fact, we observed clean Kα lines, while bremsstrahlung rays were hardly detected at all. The Kα intensity substantially increased with increases in the charging voltage.

IV. RADIOGRAPHY

The monochromatic flash radiography was performed by the CR system at 0.5 m from the x-ray source with the filter, and the charging voltage was −70 kV.

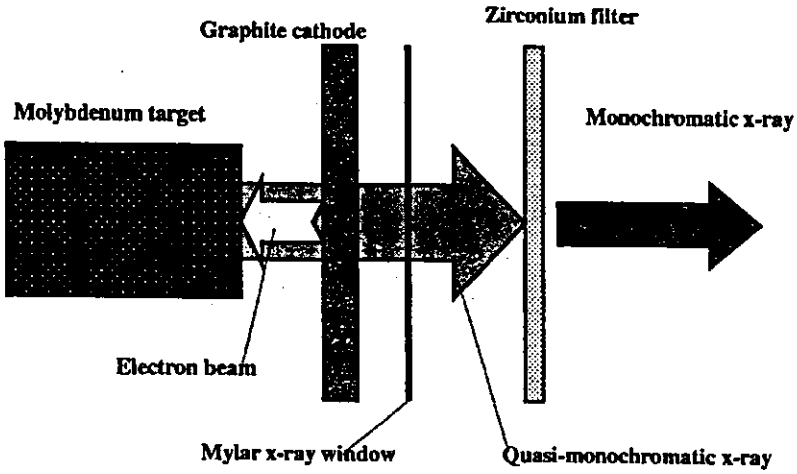

FIG. 4. Irradiation of Kα rays using a monochromatic zirconium filter. Bremsstrahlung rays are not emitted in the opposite direction to that of electron acceleration, and molybdenum Kα rays are left using a zirconium filter.

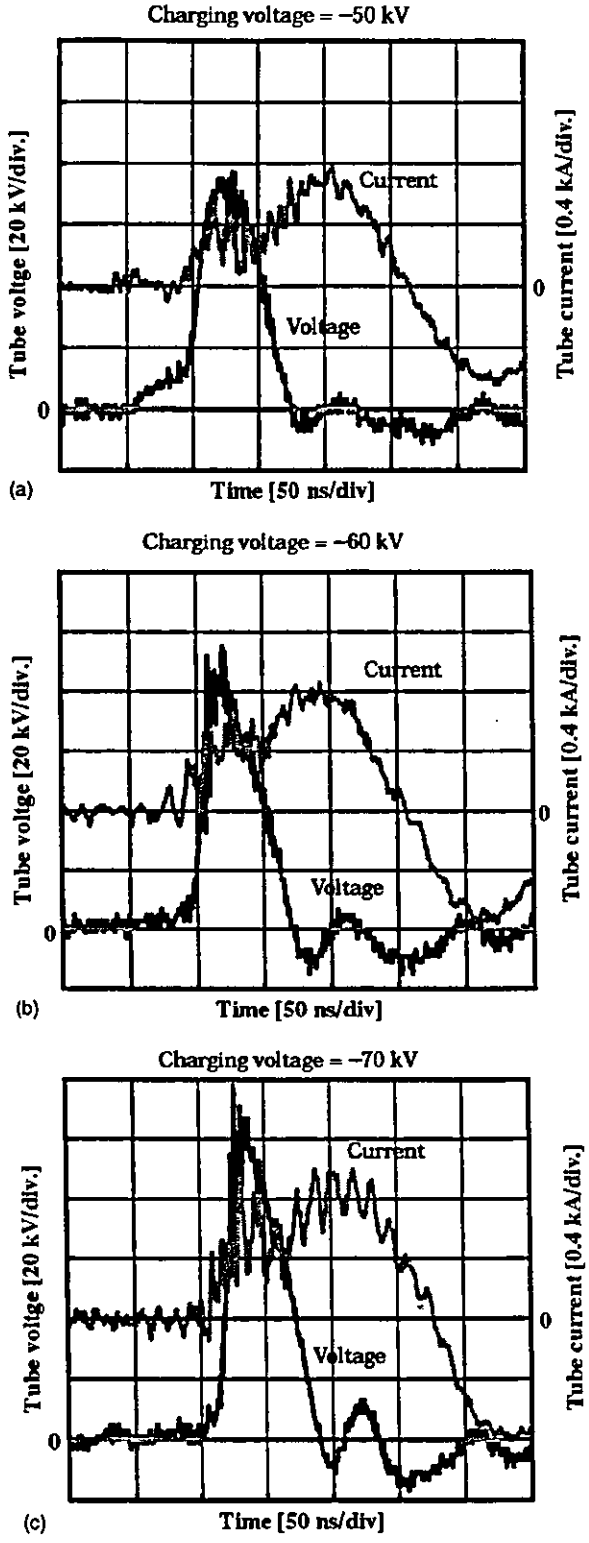

FIG. 5. Variations in the tube voltage and current with a charging voltage of (a) −50 kV, (b) −60 kV, and (c) −70 kV.

First, rough measurements of spatial resolution were made using wires. Figure 9 shows radiograms of tungsten wires coiled around a pipe made of polymethyl methacrylate. Although the image contrast increased with increases in the wire diameter, a 50 μm-diameter wire could be observed.

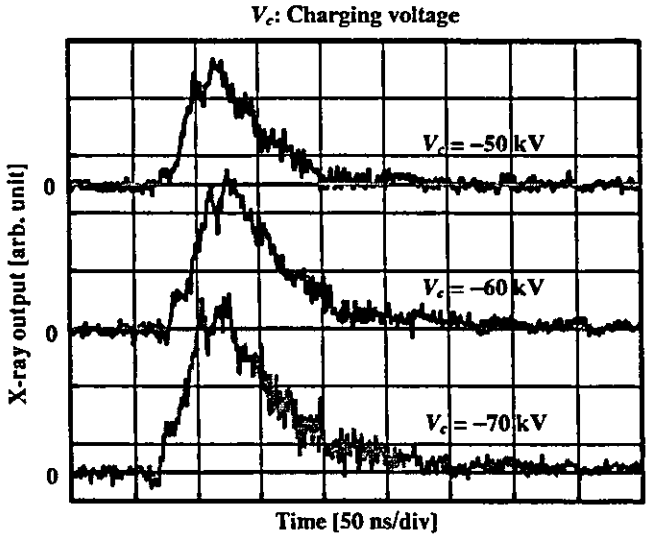

FIG. 6. X-ray outputs detected using a combination of a plastic scintillator, a photomultiplier, and the zirconium filter.

Figure 10 shows a radiogram of a vertebra, and fine structures in the vertebra were observed. Next, the image of water falling into a polypropylene beaker from a glass test tube is shown in Fig. 11. This image was taken with the slight addition of an iodine-based contrast medium. Because the x-ray duration was about 70 ns, the stop-motion image of water could be obtained. Figure 12 shows an angiogram of a rabbit heart; iodine-based microspheres of 15 μm in diameter were used, and fine blood vessels of about 100 μm were visible.

V. DISCUSSION

Concerning the spectrum measurement, we obtained fairly clean molybdenum Kα rays (17.4 keV). Therefore, we are very interested in the measurement the Kα rays from nickel (7.47 keV), copper (8.04 keV), silver (22.1 keV), cerium (34.6 keV), and tungsten (58.9 keV) targets; the target element should be selected corresponding to the radiographic objectives. In a medical application, K-series characteristic x rays of cerium are absorbed effectively by an iodine-based contrast medium with a K-edge of 33.2 keV, and high contrast microangiography can be performed.

In this research, the generator produced instantaneous number of Kα photons was approximately 3×10^7

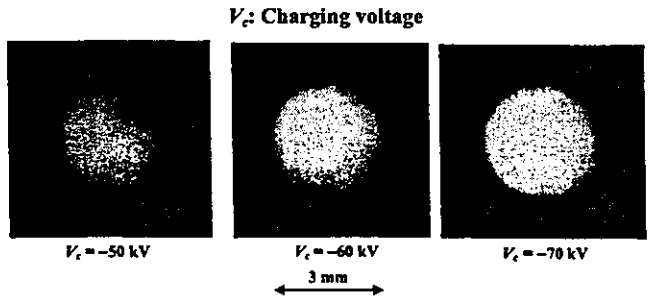

FIG. 7. Images of the x-ray source of Kα lines obtained using a pinhole camera with changes in the charging voltage.

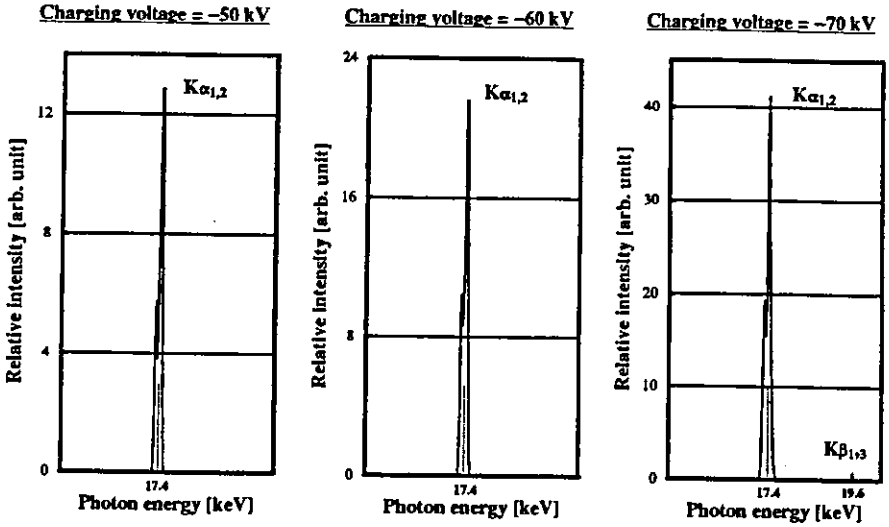

FIG. 8. X-ray spectra from the molybdenum target with the filter. The spectra were measured using a transmission type spectrometer with a lithium fluoride curved crystal.

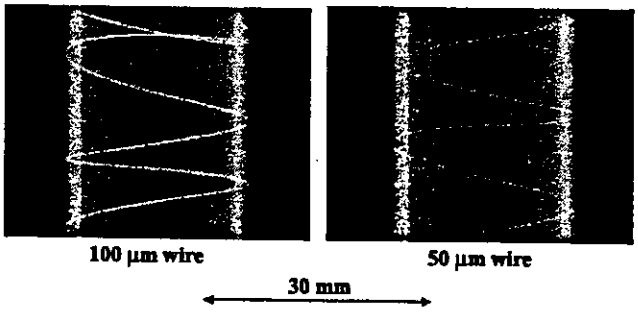

FIG. 9. Radiograms of tungsten wires of 50 and 100 μm in diameter coiled around a pipe made of polymethyl methacrylate. A 50 μm-diameter wire could be observed.

photons/cm^2 per pulse at 0.5 m from the source. Because the molybdenum plasma generator produced approximately 5 $\times 10^8$ photons/cm^2 per pulse at 1.0 m from the source, the x-ray intensity of Kα lines had a lower value as compared with the plasma x-ray generator[11] described above, which utilizes a large capacity condenser of approximately 200 nF. However, the intensity can be increased by increasing the electrostatic energy in condensers in the surge generator, and quasi-monochromatic x rays of both Kα and Kβ (19.6 keV) lines are produced without using the zirconium filter with a K-edge of 17.9 keV.

Using this flash x-ray generator, the photon energy of characteristic x rays can be selected, and we plan to design a high-speed photon-counting radiography system in order to decrease noise from radiograms. In addition, steady-state

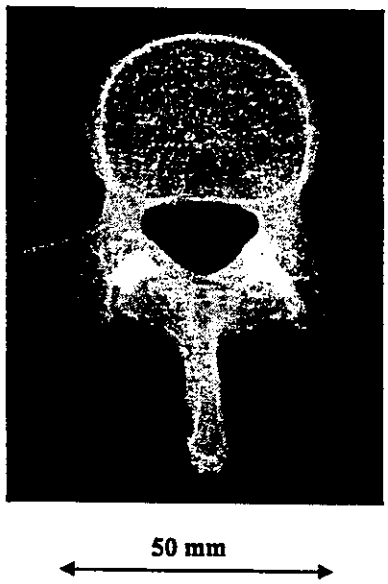

FIG. 10. Radiogram of a vertebra. Fine structure of the vertebra were visible.

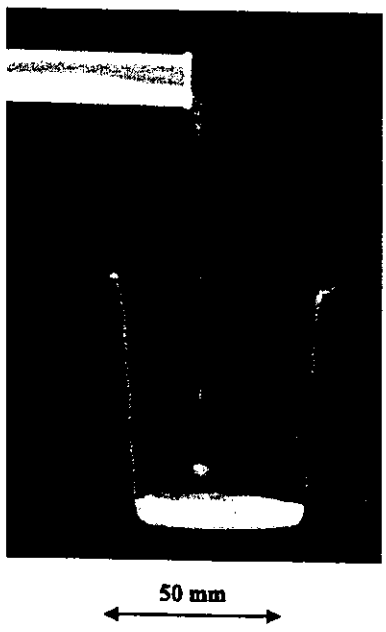

FIG. 11. Radiogram of water falling into a polypropylene beaker from a glass test tube. The stop-motion image of water was obtained by monochromatic flash radiography.

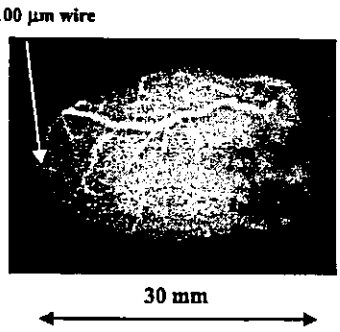

FIG. 12. Angiograms of a rabbit heart. Fine blood vessels of approximately 100 μm were visible.

monochromatic x rays for fluoroscopy can be produced by a similar tube using a constant high-voltage power supply. In conjunction with the fine focusing, these low-cost monochromatic x-ray generators will be employed to perform K-edge angiography and x-ray phase imaging for edge enhancement.[16]

ACKNOWLEDGMENTS

This work was supported by Grants-in-Aid for Scientific Research (13470154, 13877114, and 16591222) and Advanced Medical Scientific Research from MECSST, Grants from Keiryo Research Foundation, The Promotion and Mutual Aid Corporation for the Private School of Japan, JST (Test of Fostering Potential), NEDO, and MHLW (HLSRG, RAMT-nano-001, RHGTEFB-genome-005, and RGCD13C-1).

[a]Electronic mail: dresato@iwate-med.ac.jp

[1]J. J. Rocca, V. Shlyaptsev, F. G. Tomasel, O. D. Cortazar, D. Hartshorn, and J. L. A. Chilla, "Demonstration of a discharge pumped table-top soft x-ray laser," Phys. Rev. Lett. **73**, 2192–2195 (1994).

[2]J. J. Rocca, D. P. Clark, J. L. A. Chilla, and V. N. Shlyaptsev, "Energy extraction and achievement of the saturation limit in a discharge-pumped table-top soft x-ray amplifier," Phys. Rev. Lett. **77**, 1476–1479 (1996).

[3]C. D. Macchietto, B. R. Benware, and J. J. Rocca, "Generation of millijoule-level soft-x-ray laser pulses at a 4-Hz repetition rate in a highly saturated tabletop capillary discharge amplifier," Opt. Lett. **24**, 1115–1117 (1999).

[4]E. Sato, H. Isobe, and F. Hoshino, "High intensity flash x-ray apparatus for biomedical radiography," Rev. Sci. Instrum. **57**, 1399–1408 (1986).

[5]A. Shikoda, E. Sato, M. Sagae, T. Oizumi, Y. Tamakawa, and T. Yanagisawa, "Repetitive flash x-ray generator having a high-durability diode driven by a two-cable-type line pulser," Rev. Sci. Instrum. **65**, 850–856 (1994).

[6]E. Sato, K. Takahashi, M. Sagae, S. Kimura, T. Oizumi, Y. Hayasi, Y. Tamakawa, and T. Yanagisawa, "Sub-kilohertz flash x-ray generator utilizing a glass-enclosed cold-cathode triode," Med. Biol. Eng. Comput. **32**, 289–294 (1994).

[7]K. Takahashi, E. Sato, M. Sagae, T. Oizumi, Y. Tamakawa, and T. Yanagisawa, "Fundamental study on a long-duration flash x-ray generator with a surface-discharge triode," Jpn. J. Appl. Phys., Part 1 **33**, 4146–4151 (1994).

[8]E. Sato, K. Takahashi, M. Sagae, S. Kimura, T. Oizumi, Y. Hayasi, Y. Tamakawa, and T. Yanagisawa, "Sub-kilohertz flash x-ray generator utilizing a glass-enclosed cold-cathode triode," Med. Biol. Eng. Comput. **32**, 289–294 (1994).

[9]E. Sato, R. Germer, Y. Hayasi, E. Tanaka, H. Mori, T. Kawai, T. Usuki, K. Sato, H. Obara, M. Zuguchi, T. Ichimaru, H. Ojima, K. Takayama, and H. Ido, "Plasma flash x-ray generator (PFXG-02)," Proc. SPIE **4948**, 604–609 (2002).

[10]E. Sato, Y. Hayasi, R. Germer, E. Tanaka, H. Mori, T. Kwai, T. Ichimaru, K. Takayama, and Hideaki Ido, "Quasi-monochromatic flash x-ray generator utilizing weakly ionized linear copper plasma," Rev. Sci. Instrum. **74**, 5236–5240 (2003).

[11]E. Sato, Y. Hayasi, R. Germer, E. Tanaka, H. Mori, T. Kawai, H. Obara, T. Ichimaru, K. Takayama, and H. Ido, "Irradiation of intense characteristic x-rays from weakly ionized linear molybdenum plasma," Jpn. J. Med. Phys. **23**, 123–131 (2003).

[12]E. Sato, Y. Hayasi, R. Germer, E. Tanaka, H. Mori, T. Kawai, H. Obara, T. Ichimaru, K. Takayama, and H. Ido, "Intense characteristic x-ray irradiation from weakly ionized linear plasma and applications," Jpn. J. Med. Imag. Inform. Sci. **20**, 148–155 (2003).

[13]A. Mattsson, "Some characteristics of a 600 kV flash x-ray tube," Phys. Scr. **5**, 99–102 (1972).

[14]R. Germer, "X-ray flash techniques," J. Phys. E **12**, 336–350 (1979).

[15]E. Sato, K. Sato, and Y. Tamakawa, "Film-less computed radiography system for high-speed imaging," Ann. Rep. Iwate Med. Univ. Sch. Lib. Arts Sci. **35**, 13–23 (2000).

[16]A. Ishisaka, H. Ohara, and C. Honda, "A new method of analyzing edge effect in phase contrast imaging with incoherent x-rays," Opt. Rev. **7**, 566–572 (2000).

Japanese Journal of Applied Physics
Vol. 44, No. 1A, 2005, pp. 446–449

Quasi-Monochromatic X-Ray Generator Utilizing Graphite Cathode Diode with Transmission-Type Molybdenum Target

Michiaki SAGAE, Eiichi SATO, Etsuro TANAKA[1], Yasuomi HAYASI, Hidezo MORI[2], Toshiaki KAWAI[3], Toshio ICHIMARU[4], Shigehiro SATO[5], Kazuyoshi TAKAYAMA[6] and Hideaki IDO[7]

Department of Physics, Iwate Medical University, 3-16-1 Honchodori, Morioka 020-0015, Japan
[1]*Department of Nutritional Science, Faculty of Applied Bio-science, Tokyo University of Agriculture, 1-1-1 Sakuragaoka, Setagaya-ku 156-8502, Japan*
[2]*Department of Cardiac Physiology, National Cardiovascular Center Research Institute, 5-7-1 Fujishiro-dai, Suita, Osaka 565-8565, Japan*
[3]*Electron Tube Division #2, Hamamatsu Photonics K.K., 314-5 Shimokanzo, Toyooka Village, Iwata-gun 438-0193, Japan*
[4]*Department of Radiological Technology, School of Health Sciences, Hirosaki University, 66-1 Honcho, Hirosaki 036-8564, Japan*
[5]*Department of Microbiology, School of Medicine, Iwate Medical University, 19-1 Uchimaru, Morioka 020-8505, Japan*
[6]*Shock Wave Research Center, Institute of Fluid Science, Tohoku University, 2-1-1 Katahira, Aoba-ku, Sendai 980-8577, Japan*
[7]*Department of Applied Physics and Informatics, Faculty of Engineering, Tohoku Gakuin University, 1-13-1 Chuo, Tagajo 985-8537, Japan*

(Received June 19, 2004; accepted October 15, 2004; published January 11, 2005)

An X-ray generator consists of a negative high-voltage power supply and a field-emission-type cold-cathode X-ray tube. The tube is a glass-enclosed diode utilizing a transmission-type molybdenum target with a thickness of 20 μm, a needle graphite (carbon) cathode, a glass tube body, and a 0.5-mm-thick beryllium window. The tube current decreases gradually with time. After aging for 30 minutes, the tube current was approximately 0.2 mA with a tube voltage of 25 kV, and the focal-spot dimensions were 2.2 × 1.6 mm. Characteristic X-rays of molybdenum K-series were obtained after penetrating the molybdenum target and the beryllium window, and the K-absorption edge was observed clearly. The generator produced number of K photons was approximately 4×10^6 photons/cm^2·s at 1.0 m from the source. The average photon energies of Kα and Kβ lines were 17.4 and 19.6 keV, respectively, and quasi-monochromatic radiography was performed using a computed radiography system. [DOI: 10.1143/JJAP.44.446]

KEYWORDS: quasi-monochromatic X-rays, characteristic molybdenum X-rays, field emission, transmission target, quasi-monochromatic radiography

1. Introduction

Conventional medical X-ray tubes enable the observation of parts of the inside of the human body that cannot be seen by other ways. The X-ray images obtained with these tubes are exposed by both the bremsstrahlung and characteristic X-rays, unless monochromatic radiography is specifically performed. Monochromatic parallel X-ray beams are produced by synchrotrons using single crystals, and these beams have been employed to perform enhanced K-edge angiography[1–3] and X-ray phase imaging.[4,5] Subsequently, monochromatic X-ray computed tomography at two different energies has provided information on the electron density of human tissue.[6] In addition, a compact pulsed tunable monochromatic X-ray source has been designed, developed, and tested.[7] From the source, conical X-ray beams from 10 to 50 keV with pulse widths of 8 ps have been produced, and these beams are useful for biomedical imaging and protein crystallography.

Currently, flash X-ray generators[8–12] utilize cold-cathode radiation tubes and produce extremely high-dose-rate X-ray pulses with durations of less than 1 μs. In order to produce monochromatic X-rays, plasma flash X-ray generators are useful, since intense and sharp characteristic X-rays have been produced from weakly ionized linear plasmas of nickel,[13] copper[14] and molybdenum,[15] while bremsstrahlung rays are rarely detected.

In order to produce steady-state X-rays using a cold-cathode tube, the combination of the target and cathode electrodes is a very important factor. In view of the cathode, a carbon nanotube[16] is a useful field emitter and can be used as a cold cathode in an X-ray tube. Without using nanotubes, electrons can be emitted comparatively easily when lines of electric force are concentrated on a needle tip. Characteristic K-series X-rays have been obtained using a filter made of the same element as the target.

In the present research, we developed a cold-cathode X-ray tube with a needle-shaped graphite cathode, and applied it to produce characteristic molybdenum K-series X-rays by uisng a transmission target.

2. Generator

Figure 1 shows the block diagram of the X-ray generator, which consists of a negative high-voltage power supply (Model 500, −100 kV-3 mA, Pulse Electric Eng. Inc.) with dimensions of 450 × 430 × 150 mm and an X-ray tube. In the X-ray tube, the negative high voltage is applied to the cathode electrode, and the anode (target) is connected to the ground potential.

The X-ray tube is a cold-cathode diode type, as illustrated in Fig. 2. In order to perform soft radiography, including mammography, we developed a quasi-monochromatic X-ray tube with a molybdenum target. This tube consists of the following major devices: a needle-shaped graphite cathode with a tip angle of 54° and a diameter of 3.0 mm, a

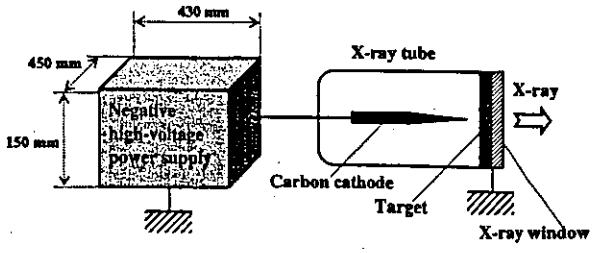

Fig. 1. Block diagram of quasi-monochromatic X-ray generator with cold-cathode diode.

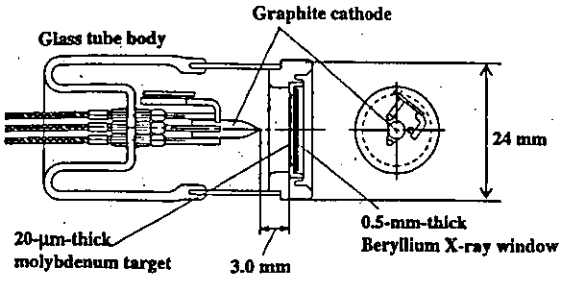

Fig. 2. Structure of X-ray tube.

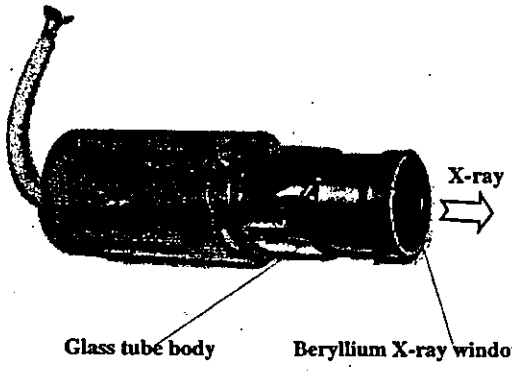

Fig. 3. Cold-cathode X-ray tube with transmission-type molybdenum target.

molybdenum disk target 20 μm thick, and a glass tube body. The target-cathode distance is 3.0 mm, and the transmission X-rays are obtained after the beam passes through the target and a 0.5-mm-thick beryllium X-ray window (Fig. 3). In this case, since the target plays the role of a K-edge filter for effectively absorbing bremsstrahlung X-rays with energies higher than the K-absorption edge, characteristic K-series X-rays are produced. The pressure in the glass-enclosed tube is primarily determined by the pressure when evacuation is stopped, and is approximately 1×10^{-4} Pa. The tube voltage is always constant and is regulated by the constant voltage power supply. Subsequently, the tube current is primarily determined by the tube voltage and the target-cathode distance, and increases with decreasing distance and increasing voltage.

In this experiment, the tube voltage applied was from 20 to 30 kV, and the exposure time was controlled in order to obtain optimum X-ray intensity for radiography.

3. Characteristics

3.1 X-ray intensity

In the field emission X-ray tube, it was very difficult to measure the X-ray intensity correctly, since the intensity gradually decreased during exposure, and small-scale vacuum breakdown may often occur. The X-ray intensity was measured using a Solidose 308 M ionization chamber for mammography at 1.0 m from the X-ray source with an exposure time of 10 s. Because the tube current increased when the tube voltage was increased, the X-ray intensity increased substantially with increasing tube voltage. In this

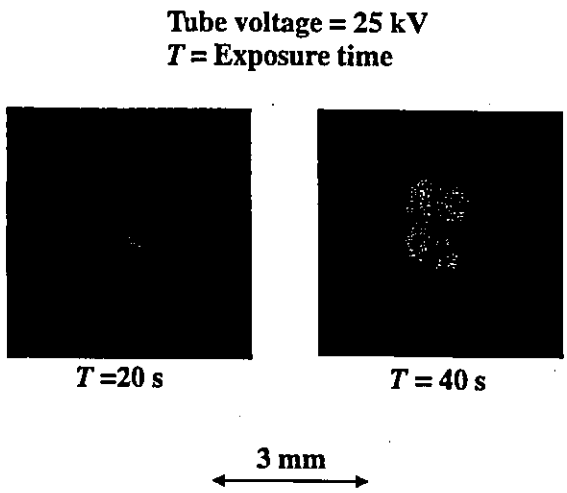

Fig. 4. Images of X-ray source with changes in exposure time.

measurement, the intensity rate with a tube voltage of 25 kV was approximately 0.3 μC/kg·s (=10 μJ/kg·s = 10 μGy/s) at 1.0 m from the source.

3.2 X-ray source

In order to measure the images of the X-ray source, we employed a pinhole camera with a hole diameter of 100 μm in conjunction with a Polaroid XR-7 (film). When the exposure time was increased with a tube voltage of 25 kV, the spot intensity increased, but the spot dimensions seldom varied and had values of 2.2 × 1.6 mm (Fig. 4).

3.3 Cathode voltage and tube current

Cathode voltage and tube current were measured using a high-voltage divider and a resistor, respectively (Figs. 5 and 6). In this generator, the cathode voltage is −1 times the tube voltage, and we observed stable cathode voltages. Thereafter, the tube current increased exponentially with increasing tube voltage in a short time. In addition, the current was unstable, and decreased gradually with time.

3.4 X-ray spectra

X-ray spectra were measured using a transmission-type spectrometer with a curved lithium fluoride crystal 0.5 mm thick. The spectra were taken using a computed radiography (CR) system (Konica Regius 150)[17] with a wide dynamic range, and relative X-ray intensity was calculated from Dicom digital data. Figure 7 shows the measured spectra from the transmission-type molybdenum target. We observed lines of characteristic K-series X-rays and K-absorption edges of molybdenum. The characteristic X-ray intensity of the Kα and Kβ lines increased substantially when the tube voltage was increased.

4. Radiography

Radiography was performed using the CR system with a sampling pitch of 87.5 μm. The distance between the X-ray source and the imaging plate was 1.0 m.

Spatial resolution was roughly measured using wires. Radiograms of tungsten wires coiled around a pipe made of polymethyl methacrylate are shown in Fig. 8. Although the

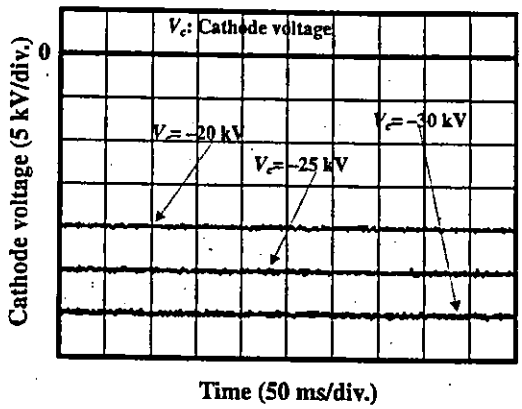

Fig. 5. Cathode voltages.

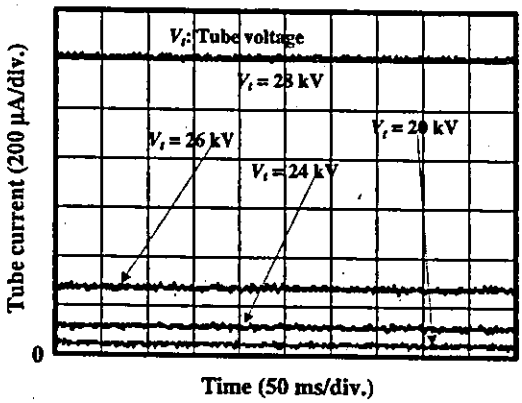

Fig. 6. Tube currents.

image contrast decreased somewhat with decreasing wire diameter due to blurring of the image caused by the sampling pitch, a 50-μm-diameter wire could be observed.

Figures 9 and 10 show angiograms of hearts. Iodine-based microspheres of 15 μm in diameter were used, and coronary

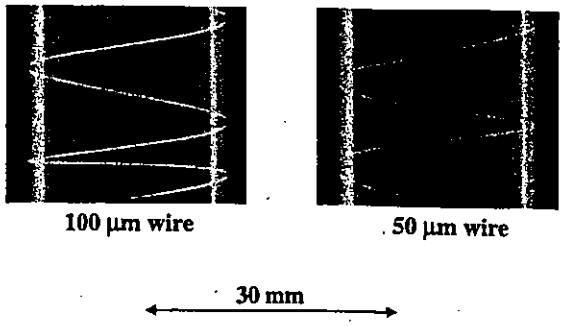

Fig. 8. Radiograms of tungsten wires of 50 and 100 μm diameter coiled around a pipe made of polymethyl methacrylate with tube voltage of 25 kV and exposure time of 20 s.

arteries and fine blood vessels of approximately 100 μm diameter were visible.

5. Discussion

In summary, we developed a simple X-ray generator with the cold-cathode diode and succeeded in producing characteristic molybdenum K-series X-rays using the transmission target as the K-edge filter. Subsequently, we confirmed the filtering effect of the target, and bremsstrahlung X-rays with photon energies higher than the edge were rarely detected with a tube voltage of 23 kV.

The current density J (A/cm^2) under field emission is written as:

$$J = 1.54 \times 10^{-6}(V/d)^2 \cdot \exp(-6.8 \times 10^7 \phi^{1.5} d/V)/\phi, \quad (1)$$

where V (V) is the tube voltage, d (cm) is the target-cathode distance, and ϕ (V) is the work function of the cathode element. Therefore, the current values in Fig. 6 corresponded qualitatively to eq. (1).

During the X-ray exposure, although the tube current decreases slightly due to ion sputtering, stable current flow can be obtained by selecting the appropriate cathode material and by controlling the radius of curvature of the cathode tip. In addition, the generator-produced number of

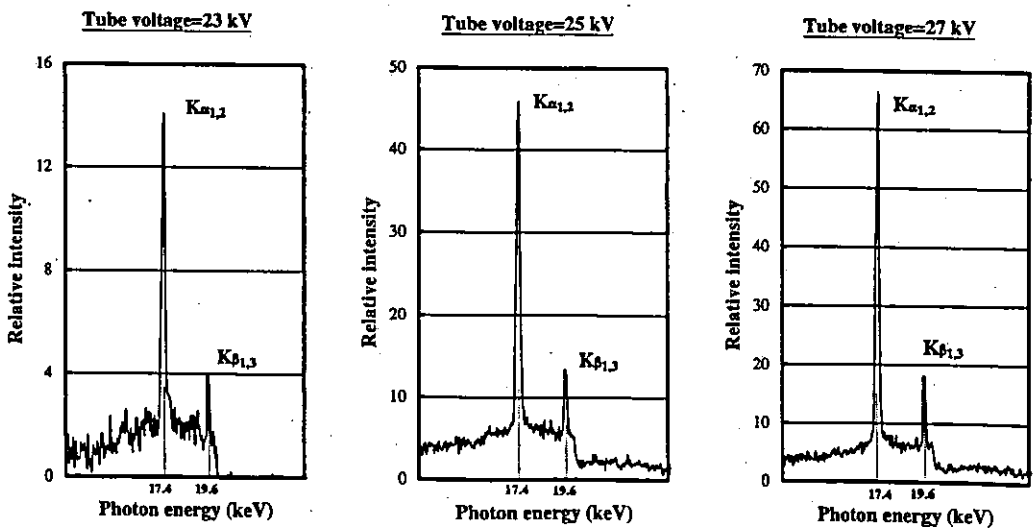

Fig. 7. X-ray spectra.